Speed and fluctuations for some driven dimer models

S. Chhita* P.L. Ferrari† F.L. Toninelli‡

Abstract

We consider driven dimer models on the square and honeycomb graphs, starting from a stationary Gibbs measure. Each model can be thought of as a two dimensional stochastic growth model of an interface, belonging to the anisotropic KPZ universality class. We use a combinatorial approach to determine the speed of growth and show logarithmic growth in time of the variance of the height function.

1 Introduction

We consider two-dimensional stochastic growth models in the anisotropic KPZ universality class [24]. Stochastic interface growth models have a random local growth mechanism which is (effectively) local in space and time, t, but with smoothing mechanisms that ensure deterministic growth under hydrodynamic scalings. In two dimensions, the average speed of growth $v(\rho)$ of the interface in a stationary state can be parameterized by the slope $\rho = (\rho_1, \rho_2)$ of the height function. The anisotropic KPZ universality class contains the models for which the signature of the Hessian of the speed of growth is $(+,-)$. This is in contrast with the usual, isotropic, KPZ universality class where the signature is $(+,+)$ or $(-,-)$. In the anisotropic case, it is expected that the fluctuations of the height function behave asymptotically like $\sqrt{\log t}$ as t grows [24]. This has been analytically verified for some exactly solvable models [3, 4, 21] and confirmed by numerical studies [11, 18]. Furthermore, it is expected that on large space-time scales and modulo a linear

*Department of Mathematical Sciences, Durham University, Stockton Road, Durham, DH1 3LE, UK. E-mail: sunil.chhita@durham.ac.uk

†Institute for Applied Mathematics, Bonn University, Endenicher Allee 60, 53115 Bonn, Germany. E-mail: ferrari@uni-bonn.de

‡Univ Lyon, CNRS, Université Claude Bernard Lyon 1, UMR 5208, Institut Camille Jordan, F-69622 Villeurbanne, France. E-mail: toninelli@math.univ-lyon1.fr

transformation of space and time coordinates, the height function fluctuations of the stationary process have the same asymptotic correlations as those found in the stochastic heat equation with additive noise (see [1, 2] for recent works).

In this paper we consider two dimer models on infinite bipartite graphs $\mathbb{Z}^2$ and $\mathcal{H}$ (the honeycomb graph). Dimers, that are viewed as particles, perform long-range jumps with asymmetric rates. For the honeycomb graph, the dynamics were defined in [4] and later extended to a partially asymmetric situation in [23]. The dynamics on $\mathbb{Z}^2$ was introduced in [23]. For both these models, translation-invariant stationary measures for interface gradients are Gibbs measures on dimer configurations with prescribed dimer densities [5, 16, 17]. In [4], the specific prescribed initial conditions were not stationary but this choice had the useful property that in a large enough subset of space-time, dimer correlation functions were determinantal. This allowed, among others, the computation of the law of large numbers and to determine that the variance of the height function behaves asymptotically like $\log t$ and has Gaussian fluctuations on that scale. However, this determinantal property for space-time correlations, which allowed for explicit computations, is no longer true for the partially asymmetric dynamics or for those with stationary initial conditions.

In this paper we consider stationary initial conditions and obtain two results, that apply equally to the totally asymmetric or to the partially asymmetric situation. The first one is the speed of growth $v^{\mathbb{Z}^2}(\rho)$ for the model on $\mathbb{Z}^2$ (Theorem 2.3). The difficulty here is to find a compact and explicit formula for the speed of growth, since by definition of the dynamics, $v^{\mathbb{Z}^2}(\rho)$ is given by an infinite sum of probabilities of certain dimer configurations and therefore by an infinite sum of determinants involving the inverse Kasteleyn matrix. To obtain this result we mimic the approach used for the honeycomb lattice in [6]. There, a combinatorial argument showed that the infinite sum reduces to a single entry of the inverse Kasteleyn matrix, leading to the explicit formula (2.5). For $\mathbb{Z}^2$, this is no longer the case, but we are able to prove that the infinite sum is given in terms of a few explicit entries of the inverse Kasteleyn matrix. As a side result, we verify explicitly that the signature of the Hessian of $v^{\mathbb{Z}^2}(\rho)$ is $(+, -)$.

The second result concerns the logarithmic growth of variance of the height function for the honeycomb graph, see Theorem 2.4 (the method can be extended to the dynamics on $\mathbb{Z}^2$ but in order not to overload this work we skip this). This result was partially proved in [23], with a technical restriction on slope ρ. Our new approach simplifies the proof contained in [23] and it extends its domain of validity to the full set of allowed slopes.

The rest of the paper is organized as follows. In Section 2 we define the models and give the results. Section 3 contains the background on dimers models. Theorem 2.3 on the speed of growth on $\mathbb{Z}^2$ is proved in Section 4. Theorem 2.4 on the variance is proved in Section 5.

Acknowledgements

F. T. was partially funded by the ANR-15-CE40-0020-03 Grant LSD, by the CNRS PICS grant "Interfaces aléatoires discrètes et dynamiques de Glauber" and by MIT-France Seed Fund "Two-dimensional Interface Growth and Anisotropic KPZ Equation". P.F. was supported by the German Research Foundation as part of the SFB 1060–B04 project. This work was supported by the LABEX MILYON (ANR-10-LABX-0070) of Université de Lyon, within the program "Investissements d'Avenir" (ANR-11-IDEX- 0007) operated by the French National Research Agency (ANR).

2 The growth models and the results

2.1 Perfect matchings and height function

We are interested in two infinite, bipartite planar graphs $\mathcal{G} = (\mathcal{V}, \mathcal{E})$ in this work: the grid $\mathbb{Z}^2$ and the honeycomb lattice $\mathcal{H}$. In both cases, we let $\mathcal{M}_\mathcal{G}$ denote the set of perfect matchings or dimer coverings of $\mathcal{G}$, i.e., subsets of edges in $\mathcal{E}$ (dimers) such that each vertex is incident to exactly one edge. Both graphs are bipartite, so we can fix a 2-coloring (say, black and white) of their vertices $\mathcal{V}$, see Figures 1 and 2. We denote $W_\mathcal{G}$ (resp. $B_\mathcal{G}$) to be the set of white (resp. black) vertices of $\mathcal{G}$.

Associated to each dimer covering $m \in \mathcal{M}_\mathcal{G}$, there is a height function h defined on faces of $\mathcal{G}$, as follows: h is fixed to zero at some given face x_0 of $\mathcal{G}$ (the "origin") and its gradients are given by

$$h(x) - h(y) = \sum_{e \in C_{x\to y}} \sigma_e(\mathbf{1}_{e\in m} - c(e)) \tag{2.1}$$

where: x, y are faces of $\mathcal{G}$, $C_{x\to y}$ is any nearest-neighbor path from x to y (the r.h.s. of (2.1) does not depend on the choice of $C_{x\to y}$), the sum runs over edges crossed by $C_{x\to y}$, σ_e equals $+1$ (resp. -1) if e is crossed with the white vertex on the right (resp. left) and $c(\cdot)$ is a function defined on the edges of $\mathcal{G}$, such that for any $v \in \mathcal{V}$,

$$\sum_{e:e\sim v} c(e) = 1, \tag{2.2}$$

where $e \sim v$ means that e is incident to v. A standard choice for the square lattice is $c(e) \equiv 1/4$; for the hexagonal lattice, we let $c(e) = 1$ if e is horizontal and $c(e) = 0$ otherwise.

As we recall in more detail in Section 3.1 below, for both graphs there exists an open polygon $P^\mathcal{G} \subset \mathbb{R}^2$ such that for every $\rho = (\rho_1, \rho_2) \in P^\mathcal{G}$ there exists a unique translation invariant and ergodic Gibbs probability measure on dimer

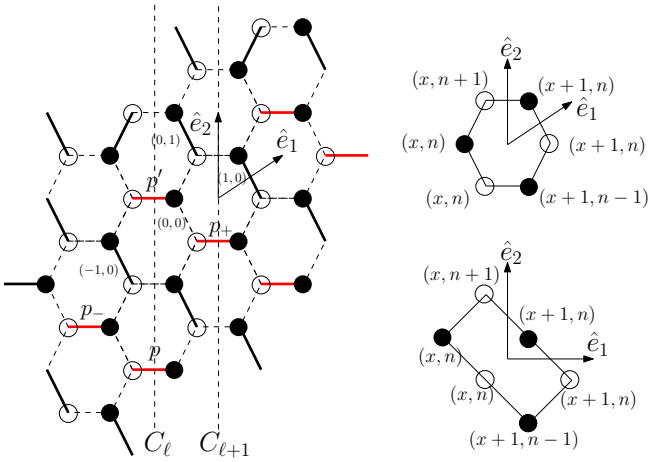

Figure 1: The left figure shows the hexagonal graph $\mathcal{H}$ with the axes $\hat{e}_1, \hat{e}_2$ and the columns C_ℓ. Coordinates (x_1, x_2) are the same for the black and white vertices on the same north-west oriented edge. Particles (i.e., horizontal dimers) are marked in red. Particles p, p' on column C_ℓ are vertically interlaced with particles $p_\pm$ on $C_{\ell\pm1}$. In Section 4.2, we will re-draw hexagonal faces as rectangular ones, as in the drawing on the right side.

coverings of $\mathcal{G}$, denoted $\pi_\rho^{\mathcal{G}}$. With the choice of coordinates we make in this work (see Section 3.1), the polygons $P^{\mathcal{G}}$ for the two graphs are as follows:

Definition 2.1. *$P^{\mathcal{H}}$ is the open triangle in $\mathbb{R}^2$ with vertices $(0,0), (0,1), (1,1)$, and $P^{\mathbb{Z}^2}$ is the open square in $\mathbb{R}^2$ with vertices $(\pm 1/2, \pm 1/2)$.*

2.2 Particles and interlacement conditions

A common feature of the two graphs $\mathbb{Z}^2$ and $\mathcal{H}$, that makes them special with respect to other planar, bipartite graphs, is that to any $m \in \mathcal{M}_{\mathcal{G}}$ one can associate a collection of "interlaced particles". First of all, we partition the set of faces of $\mathcal{G}$ into disjoint "columns" $C_\ell, \ell \in \mathbb{Z}$. In the case of $\mathcal{H}$, a column C_ℓ consists in the set of faces with the same horizontal coordinate, while for $\mathbb{Z}^2$ it is a zig-zag path as depicted in Figure 2. We call Y_ℓ the set of vertices of $\mathcal{G}$ shared by C_ℓ and $C_{\ell+1}$. Vertices $v \in Y_\ell$ can be ordered in a natural way and we will say that $v_1 < v_2$ if v_1 precedes v_2 in the upward direction (for $\mathcal{H}$) or in the up-left direction of Figure 2 (for $\mathbb{Z}^2$). An edge e of $\mathcal{G}$ will be called "transversal" if it has one endpoint on Y_ℓ and the other on $Y_{\ell+1}$ for some ℓ. Dimers on transversal edges will be called "particles".

Given two particles p and p', each with one endpoint (say v, v' respectively) on

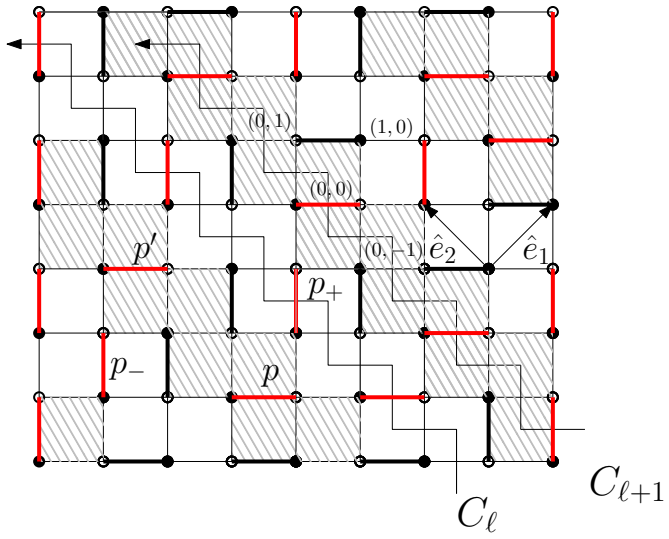

Figure 2: The square lattice $\mathbb{Z}^2$ with the axes $\hat{e}_1, \hat{e}_2$ and the "columns" C_ℓ. Coordinates (x_1, x_2) are the same for a black and the white vertex just to its right. Thick edges are dimers, and transversal dimers (or particles) are drawn in red.

the same Y_ℓ, let us say that p' is higher than p (we write $p < p'$) if $v < v'$. The following interlacement condition is easily verified both for $\mathcal{H}$ and $\mathbb{Z}^2$: given two particles p, p' on the same column C_ℓ and verifying $p < p'$, there exists a particle p_- on $C_{\ell-1}$ and a particle p_+ on $C_{\ell+1}$ such that $p < p_- < p'$, $p < p_+ < p'$. See Figures 1 and 2.

Both on $\mathbb{Z}^2$ and on $\mathcal{H}$ it is easy to check that, under the assumption that every C_ℓ contains at least one particle, the whole dimer configuration is uniquely determined by the particle configurations. In the situation we are interested in, there are almost surely infinitely many particles on each C_ℓ; therefore, we will implicitly identify a dimer configuration $m \in \mathcal{M}_\mathcal{G}$ and the corresponding particle configuration.

2.3 Dynamics and new results

We describe here the growth dynamics of [23] in a unified way for $\mathcal{G} = \mathbb{Z}^2$ and $\mathcal{G} = \mathcal{H}$. We need some preliminary notation. Given a transversal edge e on column C_ℓ, let $p(e)$ denote the highest particle in column C_ℓ that is strictly below e. Given a configuration $m \in \mathcal{M}_\mathcal{G}$, we say that "particle $p(e)$ can reach edge e" if the configuration m' obtained by moving $p(e)$ to edge e while all other particles positions are unchanged still satisfies the particle interlacement constraints, i.e., $m' \in \mathcal{M}_\mathcal{G}$.

The continuous time Markov chain of [23], in its totally asymmetric version, can be informally described as follows. To each transversal edge e of $\mathcal{G}$ is associated an i.i.d. exponential clock of mean 1. When the clock at e rings, if particle $p(e)$ can reach e without violating the interlacement constraints then it is moved there. If $p(e)$ cannot reach e, then nothing happens.

Note that the size of particle jumps are unbounded, so it is not a-priori obvious that the definition of the Markov process is well-posed. However, one of the results of [23] is that given any $\rho \in P^{\mathcal{G}}$, for almost every initial condition sampled from the Gibbs measure $\pi_\rho^{\mathcal{G}}$ the dynamics is well-defined (i.e., almost surely no particle travels an infinite distance in finite time). Also, it is proved there that the measures $\pi_\rho^{\mathcal{G}}$ are stationary for the dynamics. We let $\nu_\rho^{\mathcal{G}}$ denote the law of the stationary process started from $\pi_\rho^{\mathcal{G}}$.

Note that when $p(e)$ is moved from its current position in column say C_ℓ to the edge e in the same column, it jumps over a certain number $n \geq 1$ of faces of C_ℓ. We define the "integrated current" $J(t)$ as the total number of particles that jump across a given face of the graph, say across the face x_0 that was chosen as origin, from time 0 to time t ($J(t)$ is a multiple of the height change at x_0). In [23] it was proven:

Theorem 2.2. *For every $\rho \in P^{\mathcal{G}}$, there exists $v^{\mathcal{G}}(\rho) > 0$ such that*

$$\nu_\rho^{\mathcal{G}}(J(t)) = t v^{\mathcal{G}}(\rho). \tag{2.3}$$

Moreover, if $\mathcal{H} = \mathcal{G}$ then there exists a non-empty subset of $A \subset P^{\mathcal{G}}$ such that, for every $\rho \in A$,

$$\limsup_{t\to\infty} \frac{\mathrm{Var}_{\nu_\rho^{\mathcal{G}}}(J(t))}{\log t} < \infty. \tag{2.4}$$

Later, in [6], the function $v^{\mathcal{G}}(\rho)$ for $\mathcal{G} = \mathcal{H}$ was computed explicitly[1]:

$$v^{\mathcal{H}}(\rho) = \frac{1}{\pi} \frac{\sin(\pi\rho_1)\sin(\pi(\rho_2 - \rho_1))}{\sin(\pi\rho_2)}. \tag{2.5}$$

Our main results here complete the above picture as follows:

Theorem 2.3. *For the dynamics on $\mathbb{Z}^2$, the speed of growth is given by*

$$v^{\mathbb{Z}^2}(\rho) = \frac{1}{\pi} \sin\psi_1 \left(\frac{\sin\psi_1}{\tan\psi_2} + \sqrt{1 + \frac{\sin^2\psi_1}{\tan^2\psi_2}} \right) \tag{2.6}$$

where $\psi_i = (\rho_i + 1/2)\pi$ for $i \in \{1, 2\}$ takes value in $[0, \pi]$.

[1] In this work we use different conventions as in [23] for lattice coordinates and this is the reason why formula (2.5) looks different from formula (3.6) of [23]

It is immediate to see that the r.h.s. of (2.5) (resp. of (2.6)) is positive in the whole triangle $P^{\mathcal{H}}$ (resp. in the square $P^{\mathbb{Z}^2}$) of Definition 2.1.

Theorem 2.4. *For $\mathcal{G} = \mathcal{H}$, (2.4) holds for every $\rho \in P^{\mathcal{G}}$.*

Moreover, the proof of (2.4) we give here is substantially simplified w.r.t. the one in [23]. Also, our method can be easily adapted to prove Theorem 2.4 also for the dynamics on $\mathbb{Z}^2$ and every $\rho \in P^{\mathbb{Z}^2}$ but, in order to keep this work within a reasonable length, we do not give details on this extension.

Remark 2.5. *From the above explicit expression (2.6) it is possible to check (see Appendix B) that the Hessian of the function $\rho \mapsto v^{\mathbb{Z}^2}(\rho)$ has signature $(+,-)$ for every $\rho \in P^{\mathbb{Z}^2}$. This means that our model belongs to the anisotropic KPZ universality class.*

Remark 2.6. *The work [23] studies a more general, partially asymmetric dynamics where upward jumps have rate p and downward jumps have rate q. In this case, the speed of growth is given by the above formulas multiplied by $p-q$. Also, the result on the variance holds true also for the partially asymmetric version. In fact, from [23, Sec. 9] one sees that Theorem 2.4 holds for general p, q as soon as Theorem 3.1 below, that is independent of p, q, is proved.*

2.4 Geometric interpretation of $v^{\mathcal{G}}(\rho)$

The stationary and translation invariant Gibbs measures form a two-parameter family. From an interface perspective, it is natural to use the average slope of the interface, $\rho = (\rho_1, \rho_2)$, as parametrization. Then all other quantities, such as the average number of dimers of a given type or the speed of growth, are functions of ρ. As it was already known for the honeycomb lattice, the correlation kernel giving dimer correlations, that in principle is a double contour integral [17], can be rewritten as a single integral from $\overline{\Omega}_c$ to Ω_c, where $\Omega_c = \Omega_c(\rho)$ is a complex number in the upper half plane $\mathbb{H}$. Further, for $\mathcal{G} = \mathcal{H}$ and for a special initial condition, it was shown [4] that the height field fluctuations of the growth model converges to a Gaussian free field (GFF). More precisely, the correlations on a macroscopic scale at m different points converge to the correlations of the GFF on $\mathbb{H}$ between the points obtained by mapping the m points to $\mathbb{H}$ by Ω_c. The map Ω_c was known already from the work of Kenyon [15] (there it is called Φ in Section 1.2.3 and Figure 2). A generalization of [4] to a setting with two different jump rates was made in [10].

Here we shortly present how the densities of the different types of dimers, the correlation kernel and the speed of growth are written in terms of Ω_c. For the hexagonal lattice we refer to [4]: the three types of dimers are in Figure 5.1, the

points 0, 1 and Ω_c form a triangle whose internal angles are π times the frequencies of the types of dimers (Figure 3.1), and the correlation kernel as a single integral is given in [4, Prop. 3.2]. Finally, an interesting property is that the speed of growth (2.5) equals $\frac{1}{\pi}\mathrm{Im}(\Omega_c)$.

For the square lattice, there also exists $\Omega_c = \Omega_c(\rho) \in \mathbb{H}$ (not the same one as for the hexagonal lattice) such that the correlation kernel is given as a single integral from $\overline{\Omega}_c$ to Ω_c (see Lemma A.1). Using this and formula (3.2) below, one can easily compute the densities of the different types of dominoes with the result

$$\begin{aligned} a_1 &= \text{density of } (\bullet(0,0), \circ(0,0)) = \frac{1}{\pi}\left[\arg(\Omega_c) - \arg(\Omega_c + 1)\right], \\ a_2 &= \text{density of } (\bullet(0,0), \circ(0,1)) = \frac{1}{\pi}\left[\arg(\Omega_c - 1) - \arg(\Omega_c)\right], \\ a_3 &= \text{density of } (\bullet(0,0), \circ(-1,1)) = 1 - \frac{1}{\pi}\arg(\Omega_c - 1), \\ a_4 &= \text{density of } (\bullet(0,0), \circ(-1,0)) = \frac{1}{\pi}\arg(\Omega_c + 1). \end{aligned} \tag{2.7}$$

Further, the slopes are given (see (3.8)-(3.9) and Lemma A.2) by

$$\begin{aligned} \rho_1 + \tfrac{1}{2} &= \frac{1}{\pi}\arg(\Omega_c) = a_1 + a_4 = 1 - a_2 - a_3, \\ \rho_2 + \tfrac{1}{2} &= \frac{1}{\pi}\left[\arg(\Omega_c - 1) - \arg(\Omega_c + 1)\right] = a_1 + a_2 = 1 - a_3 - a_4. \end{aligned} \tag{2.8}$$

Finally, it follows from Appendix A that the speed of growth (2.6) is given by

$$v^{\mathbb{Z}^2}(\rho) = \frac{1}{\pi}\mathrm{Im}(\Omega_c), \tag{2.9}$$

which, remarkably, is the same form as in the hexagonal case. As in the hexagonal case, also in the square case $\Omega_c(\rho)$ has a nice geometric representation in terms of dimer densities, see Figure 3.

3 Background

3.1 Gibbs Measures

An ergodic Gibbs measure or simply a Gibbs measure π, in our context, is a probability measure on $\mathcal{M}_{\mathcal{G}}$ that is invariant and ergodic w.r.t. translations in $\mathcal{G}$ and satisfies the following form of DLR (Dobrushin-Lanford-Ruelle) equations: for any finite subset of edges Λ, the law $\pi(\cdot|m_{\Lambda^c})$ conditioned on the dimer configuration on edges not in Λ is the uniform measure on the finitely many dimer configurations

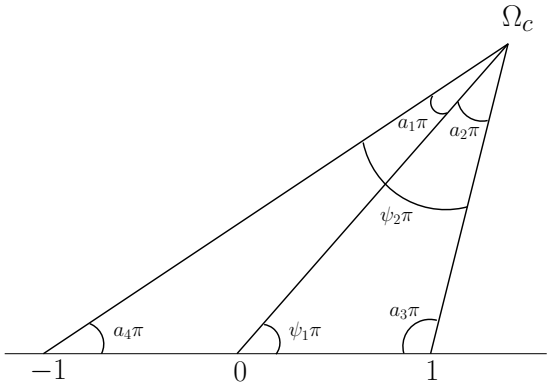

Figure 3: Geometric interpretation of Ω_c in terms of slopes and dimers densities. Here $\psi_i = \rho_i + 1/2$.

on Λ that are compatible with m_{Λ^c}. By translation invariance, to a Gibbs measure one can associate an average slope $\rho = (\rho_1, \rho_2)$, such that

$$\pi(h(x + \hat{e}_i) - h(x)) = \rho_i, \quad i = 1, 2, \tag{3.1}$$

with $\hat{e}_i$ the coordinate unit vectors.

It is convenient, both for this section and the rest of the work, to make an explicit choice of coordinates on $\mathcal{G}$. Let us start with the graph $\mathcal{H}$. Both white and black vertices are assigned coordinates $x = (x_1, x_2) \in \mathbb{Z}^2$. The two (white and black) endpoints of the same north-west oriented edge will be assigned the same coordinates (we will denote them $\circ(x_1, x_2), \bullet(x_1, x_2)$) and we make an arbitrary choice of which edge has endpoints of coordinates $(0, 0)$. The coordinate vectors $\hat{e}_1, \hat{e}_2$ are chosen to be the unit vectors forming an angle $\pi/6$ and $\pi/2$, respectively, w.r.t. the horizontal axis. See Figure 1. Note that the nearest neighbors of the black vertex $\bullet(0, 0)$ are the white vertices $\circ(0, 0), \circ(0, 1)$ and $\circ(-1, 1)$.

As for $\mathbb{Z}^2$, we let $\hat{e}_1, \hat{e}_2$ be the vectors forming an angle $\pi/4$ and $3\pi/4$ w.r.t. the horizontal axis, see Figure 2. Again we fix arbitrarily the origin of the lattice and we establish that a white vertex has the same coordinates (x_1, x_2) as the black vertex just to its left. The nearest neighbors of the black vertex $\bullet(0, 0)$ are the white vertices $\circ(0, 0), \circ(0, 1), \circ(-1, 1), \circ(-1, 0)$.

Recalling the definition of height function it is easy to see that, for any Gibbs measure π, the slope ρ must belong to the closure of the polygon $P^{\mathcal{G}}$ of Definition 2.1.

It is known [17] that for every $\rho \in P^{\mathcal{G}}$ there exists a unique Gibbs measure $\pi := \pi^{\mathcal{G}}_{\rho}$ with slope ρ. This can be obtained as the limit (as $L \to \infty$) of the uniform measure on the subset of dimer coverings of the $L \times L$ periodization of the

lattice $\mathcal{G}$ such that the height function changes by $\lfloor L\rho_i \rfloor$ along a cycle in direction $\hat{e}_i, i = 1, 2$.

The correlations of the measure $\pi_\rho^{\mathcal{G}}$ have a determinantal representation [17], that we briefly recall here. First of all, one needs to introduce the Kasteleyn matrix: this is the infinite, translation invariant, matrix $\left[\bar{K}(b,w)\right]_{b\in B_{\mathcal{G}}, w\in W_{\mathcal{G}}}$, with rows/columns indexed by black/white vertices of $\mathcal{G}$. Matrix elements are non-zero complex numbers for b, w nearest neighbors and are zero otherwise. The non-zero elements depend also on the slope ρ. See below for the explicit expression of $\bar{K}$ for the graphs $\mathcal{H}$ and $\mathbb{Z}^2$. Next, one introduces an infinite, translation-invariant matrix $\left[\bar{K}^{-1}(w,b)\right]_{w\in W_{\mathcal{G}}, b\in B_{\mathcal{G}}}$ (as the notation suggests, $\bar{K}\bar{K}^{-1}$ equals the identity matrix). Again, see below for the expression of $\bar{K}^{-1}$ for $\mathcal{G} = \mathcal{H}$ and $\mathcal{G} = \mathbb{Z}^2$. All multi-point correlations of $\pi_\rho^{\mathcal{G}}$ can be expressed via $\bar{K}$ and $\bar{K}^{-1}$ as follows [17]: given edges $e_i = (w_i, b_i), i \leq k$,

$$\pi_\rho^{\mathcal{G}}(e_1, \dots, e_k \in m) = \left(\prod_{i=1}^{k} \bar{K}(b_i, w_i) \right) \det[\bar{K}^{-1}(w_i, b_j)]_{1\leq i,j\leq k}. \tag{3.2}$$

The definition of matrices $\bar{K}, \bar{K}^{-1}$ is not unique and different choices than the one we make below can be found in the literature.

For $\mathcal{G} = \mathcal{H}$, we let

$$\overline{K}(b,w) = \begin{cases} a_2 & \text{if } b = \bullet(x_1,x_2), w = \circ(x_1,x_2), \\ a_1 & \text{if } b = \bullet(x_1,x_2), w = \circ(x_1-1,x_2+1), \\ a_3 & \text{if } b = \bullet(x_1,x_2), w = \circ(x_1,x_2+1), \end{cases} \tag{3.3}$$

where $a_i = a_i(\rho) > 0$ are such that in the triangle with sides a_1, a_2, a_3, the angle opposite to the side of length a_i is $\pi r_i > 0$, with $r_1 = 1 - \rho_2$, $r_2 = \rho_1$ and $r_3 = \rho_2 - \rho_1$. Note that r_1 (resp. r_2, r_3) is the density of dimers oriented horizontally (resp. oriented north-west, north-east). The inverse Kasteleyn matrix $\overline{K}^{-1}$ is

$$\overline{K}^{-1}(w,b) = \frac{1}{(2\pi \mathrm{i})^2} \int dz_1 dz_2 \frac{z_1^{y_2-x_2} z_2^{x_2-y_2+x_1-y_1-1}}{a_1 + a_2 z_1 + a_3 z_2}, \tag{3.4}$$

with $w = \circ(x_1, x_2)$ and $b = \bullet(y_1, y_2)$ and the integral runs over the anticlockwise circles $|z_1| = |z_2| = 1$ in the complex plane.

For $\mathcal{G} = \mathbb{Z}^2$ we take instead

$$\overline{K}(b,w) = \begin{cases} \mathrm{i}e^{B_1} & \text{if } b = \bullet(x_1,x_2), w = \circ(x_1,x_2), \\ e^{B_1+B_2} & \text{if } b = \bullet(x_1,x_2), w = \circ(x_1,x_2+1), \\ \mathrm{i}e^{B_2} & \text{if } b = \bullet(x_1,x_2), w = \circ(x_1-1,x_2+1), \\ 1 & \text{if } b = \bullet(x_1,x_2), w = \circ(x_1-1,x_2), \end{cases} \tag{3.5}$$

(the "magnetic fields" B_1, B_2 are fixed by the slope ρ as specified below) and the inverse Kasteleyn matrix $\overline{K}^{-1}$ is given by

$$\overline{K}^{-1}(w,b) = \frac{1}{(2\pi \mathrm{i})^2} \int \frac{dz_1}{z_1} \frac{dz_2}{z_2} \frac{z_1^{y_1-x_1} z_2^{y_2-x_2}}{\mu(z_1,z_2)}, \quad w = \circ(x_1,x_2), b = \bullet(y_1,y_2) \tag{3.6}$$

where the integral runs over $|z_1| = |z_2| = 1$ and

$$\mu(z_1,z_2) = z_1(1 + e^{B_1}\mathrm{i}z_1^{-1} + e^{B_2}\mathrm{i}z_2^{-1} + e^{B_1+B_2}z_1^{-1}z_2^{-1}), \tag{3.7}$$

The parameters $B = (B_1, B_2)$ are related to the slope $\rho = (\rho_1, \rho_2)$ as follows:

$$\rho_1 = \rho_1(B) = \frac{1}{2} - \left(\mathrm{i}e^{B_2}\overline{K}^{-1}(\circ(-1,1), \bullet(0,0)) + e^{B_1+B_2}\overline{K}^{-1}(\circ(0,1), \bullet(0,0))\right) \tag{3.8}$$

and

$$\rho_2 = \rho_2(B) = -\frac{1}{2} + \left(\mathrm{i}e^{B_1}\overline{K}^{-1}(\circ(0,0), \bullet(0,0)) + e^{B_1+B_2}\overline{K}^{-1}(\circ(0,1), \bullet(0,0))\right). \tag{3.9}$$

This is simply because, by the definition of height function, one has for instance

$$\rho_1 = 1/2 - \pi_\rho^{\mathbb{Z}^2}((\circ(-1,1), \bullet(0,0)) \in m) - \pi_\rho^{\mathbb{Z}^2}((\circ(0,1), \bullet(0,0)) \in m) \tag{3.10}$$

and then (3.8) follows from (3.2). It is known [17] that the relations (3.8), (3.9) given a bijection between $P^{\mathbb{Z}^2}$ and the "amoeba"

$$\mathcal{B} = \{B : |\sinh(B_1)\sinh(B_2)| < 1\} = \{B : |\tanh(B_2)\cosh(B_1)| < 1\}. \tag{3.11}$$

Injectivity of the map $B \mapsto \rho(B)$ is related to the fact that (ρ_1, ρ_2) is the gradient w.r.t. (B_1, B_2) of a surface tension function that is a convex function of (B_1, B_2).

3.2 Average and variance of the current

For ease of notation, given distinct edges $e_1, \dots e_{n+k}$ of $\mathcal{G}$, we let

$$\pi_\rho^{\mathcal{G}}(e_1, \dots, e_n, e_{n+1}^c, \dots, e_{n+k}^c) := \pi_\rho^{\mathcal{G}}(e_i \in m \ \forall i \le n, \ e_{n+i} \notin m \ \forall i \le k) \tag{3.12}$$

where we recall that m denotes the dimer covering.

3.2.1 Average current

Let ℓ_0 denote the index such that the face x_0 of $\mathcal{G}$ that we established to be the origin is in column C_{ℓ_0} and let S denote the set of edges e, transversal to C_{ℓ_0}, that

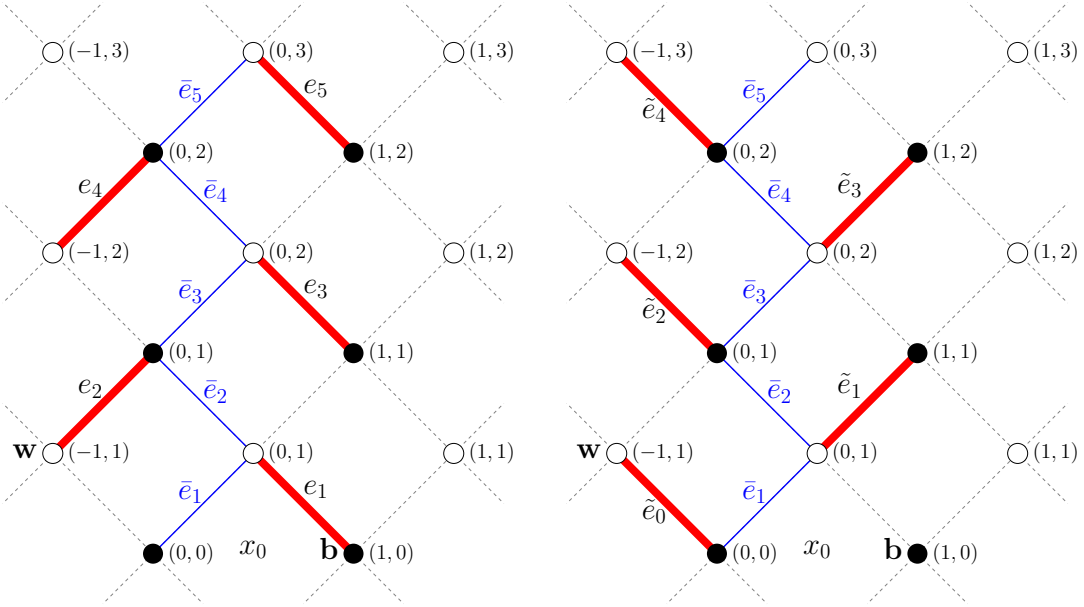

Figure 4: The left figure shows the edges $e_1, e_2, \ldots$, etc., which are shown with solid red lines. The right figure shows the edges $\tilde{e}_0, \tilde{e}_1, \ldots$, etc., which are showed with solid red lines.

are above x_0. Then, from the definition of the dynamics, we obtain the following expression for the speed $v^{\mathcal{G}}(\rho)$:

$$v^{\mathcal{G}}(\rho) = \sum_{e \in S} \pi_\rho^{\mathcal{G}}(U(e)) := \sum_{e \in S} \pi_\rho^{\mathcal{G}}(p(e) \text{ is below } x_0 \text{ and can reach edge } e) \quad (3.13)$$

simply because, if $p(e)$ can reach e, it will do so with rate 1 and with such an update, it will increase the integrated current $J(t)$ through x_0 by 1.

Then, (3.13) can be expressed more explicitly. In view of Theorem 2.3, we consider the case $\mathcal{G} = \mathbb{Z}^2$. With reference to Figure 4, where for convenience we rotated the graph by $\pi/4$ clockwise, we first notice that S consists of the set of transversal edges $\{\bar{e}_i\}_{i \geq 1}$. Also, it is easily checked that the event $U(\bar{e}_1)$ is equivalent to the event that edge e_1 is occupied by a dimer while $\tilde{e}_0$ is not. Finally, the event $U(\bar{e}_i)$, $i \geq 2$, is equivalent to the event that edges $e_1, \ldots, e_i$ are all occupied by dimers.

As a consequence,

$$v^{\mathbb{Z}^2}(\rho) = \pi_\rho^{\mathbb{Z}^2}(e_1, \tilde{e}_0^c) + \sum_{n \geq 2} \pi_\rho^{\mathbb{Z}^2}(e_1, \ldots, e_n). \quad (3.14)$$

In Section 4 we will show that the r.h.s. of (3.14) equals the r.h.s. of (2.6). The sum is convergent: in fact, label $x_i, i \geq 0$ the faces in the column C_{ℓ_0}, where x_i

is adjacent to and above x_{i-1}. Then, the event $\{e_1, \dots, e_n \in m\}$ is equivalent to $h(x_n) - h(x_0) = -n/2$. On the other hand, $\pi_\rho^{\mathbb{Z}^2}(h(x_n) - h(x_0)) = n\rho_2$ so that

$$\pi_\rho^{\mathbb{Z}^2}(e_1, \dots, e_n) = \pi_\rho^{\mathbb{Z}^2}\left[h(x_n) - h(x_0) - \pi_\rho^{\mathbb{Z}^2}(h(x_n) - h(x_0)) = -n(\rho_2 + 1/2)\right]. \tag{3.15}$$

Observe that $\rho_2 > -1/2$ since $\rho \in P^{\mathbb{Z}^2}$. Finally, since the k^{th} centered moment of $h(x_n) - h(x_0)$ is $\mathcal{O}((\log n)^{k/2})$ [19, App. A] the summability of (3.14) follows.

3.2.2 Variance of the current

Let us move to the variance of $J(t)$ for $\mathcal{G} = \mathcal{H}$ (we do not work out formulas for $\mathcal{G} = \mathbb{Z}^2$). Recall that, given a dimer configuration $m \in \mathcal{M}_\mathcal{H}$ and a horizontal edge e, we denote $p(e)$ the highest particle below e in the same column. We denote $V(e)$ the number hexagonal faces that $p(e)$ has to cross in order to reach edge e and we set $V(e) = 0$ if $p(e)$ cannot be moved to e (i.e., if the move violates interlacements).

Going back to [23, Sec. 9 and Appendix A], one sees that to prove Theorem 2.4 it is sufficient to show:

Theorem 3.1. *Denote by Λ_L the set of horizontal edges $e = (\bullet(x+1, n), \circ(x, n+1))$ with $0 \le x \le L, 0 \le n \le L$. Then, for every $\rho \in P^\mathcal{H}$ there exists a constant c such that*

$$\mathrm{Var}_{\pi_\rho}\left(\sum_{e \in \Lambda_L} V(e)\right) \le cL^2 \log L. \tag{3.16}$$

3.3 Dimer coverings of bipartite graphs

In the following, we will need more general bipartite graphs $G = (V, E)$ than just $\mathbb{Z}^2$ and $\mathcal{H}$. To each of the edges $e \in E$, we assign a positive number called an *edge weight*. We denote the weight of the edge e by $\omega(e)$ with $\omega : E \to \mathbb{R}_{>0}$. We denote the set of dimer coverings by $\mathcal{M}_G$ and, if the graph is finite, we denote the partition function by Z_G. That is,

$$Z_G = \sum_{m \in \mathcal{M}_G} \prod_{e \in m} \omega(e). \tag{3.17}$$

We define $\mathbb{P}_G$ to be the dimer model probability measure on the graph G, that is for $m \in \mathcal{M}_G$, $\mathbb{P}_G(m) = \prod_{e \in m} \omega(e)/Z_G$.

Definition 3.2. *Given a subset of edges $E_1 \subset E$ and a subset of vertices $V_1 \subset V$, we write $G \backslash \{E_1, V_1\}$ to be the graph G with all the edges in E_1 and vertices in V_1 removed from G, along with the edges incident to either V_1 or E_1. Let $Z_G[E_1, V_1]$ denote the partition function of this graph (if either E_1 or V_1 is empty we omit it from the notation).*

We use K_G to denote the *Kasteleyn matrix* of G which has columns indexed by the black vertices and rows indexed by white vertices with entries given by

$$(K_G)_{bw} = \begin{cases} \operatorname{sign}(e)\omega(e) & \text{if } e=(b,w) \text{ is an edge,} \\ 0 & \text{if } w \text{ and } b \text{ are not connected by an edge,} \end{cases} \tag{3.18}$$

where $\operatorname{sign}(e)$ is a modulus-one complex number chosen so as to satisfy the following property. Given a face f of the graph, let $e_1, \ldots, e_{2n}$ be the edges incident to it, ordered say clockwise with an arbitrary choice for e_1. Then, we impose that

$$\Phi(f) := \frac{\operatorname{sign}(e_1)\operatorname{sign}(e_3)\ldots\operatorname{sign}(e_{2n-1})}{\operatorname{sign}(e_2)\operatorname{sign}(e_4)\ldots\operatorname{sign}(e_{2n})} = (-1)^{n+1}. \tag{3.19}$$

This is called a *Kasteleyn orientation*. Existence of a Kasteleyn orientation for every (bipartite) planar graph is known [12] and in general many choices are possible. When G is a bipartite sub-graph of the infinite lattice $\mathcal{G} = \mathbb{Z}^2$ or $\mathcal{H}$ and $e = (b, w)$, the restriction of $\bar{K}$ to G *does not* in general provide a correct Kasteleyn orientation for G and this will be an important point later.

Kasteleyn [12, 13] and independently Temperley and Fisher [22] noticed that $Z_G = |\det K_G|$ for domino tilings (to be more precise, their formulations involved the more complicated non-bipartite graphs but the above formulation is sufficient for this paper). This identity is true irrespective of the choice of Kasteleyn orientation and holds for any bipartite finite planar graph. An observation due to Kenyon [14] shows that statistical properties can be found using the inverse of the Kasteleyn matrix, that is, for $e_1 = (b_1, w_1), \ldots, e_m = (b_m, w_m)$ edges in the graph G,

$$\mathbb{P}_G(e_1, \ldots, e_m) = \left(\prod_{i=1}^{m} K(b_i, w_i) \right) \det[K^{-1}(w_i, b_j)]_{1 \le i,j \le m}. \tag{3.20}$$

Actually, the analogous formula (3.2) for the infinite graph is obtained from (3.20) by suitably letting G tend to the infinite graph $\mathcal{G}$ by toroidal exhaustion [17].

Remark 3.3. *Given an edge weight function $\omega : e \in E \mapsto \omega(e) > 0$, define face weights as the alternating product of the edge weights: given a face f of G adjacent to edges $e_1, \ldots, e_{2n}$ (say in clockwise order with a given choice of e_1), let*

$$\omega(f) = [\omega(e_1)\omega(e_3)\ldots\omega(e_{2n-1})]/[\omega(e_2)\omega(e_4)\ldots\omega(e_{2n})]. \tag{3.21}$$

The dimer model probability measure is uniquely parametrized by its face weights, which means that two edge weight functions lead to the same probability measure if the corresponding face weights are equal. Suppose that ω_1 and ω_2 are two such edge weight functions. Then there exist functions $F_\circ$ and $F_\bullet$ on white and black vertices respectively such that $\omega_1(e)/\omega_2(e) = F_\circ(w)F_\bullet(b)$ for each edge $e = (w, b)$.

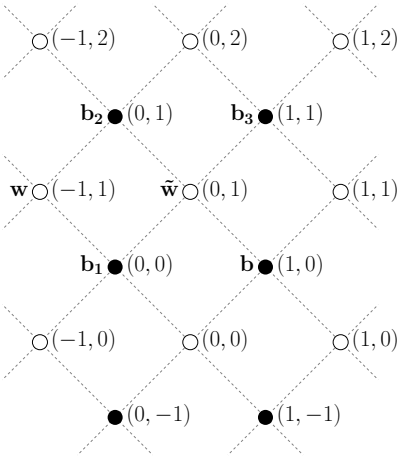

Figure 5: The coordinate system used for square grid with the vertices $\mathbf{w}$, $\tilde{\mathbf{w}}$, $\mathbf{b}$, $\mathbf{b_1}$, $\mathbf{b_2}$ $\mathbf{b_3}$ and $\mathbf{b_4}$.

We say that ω_1 and ω_2 are gauge equivalent and the act of multiplying edge weights by functions defined on its incident vertices is called a gauge transformation. The Kasteleyn matrix for a gauge equivalent weighting is obtained by pre-and post-composing with diagonal matrices built from the gauge transformation functions.

4 Speed of growth on $\mathbb{Z}^2$

In this section, we prove (2.6). We begin by remarking that the edges $e_{2m+1}, m \geq 0$ that appear in formula (3.14) are the edges $(\bullet(1,m), \circ(0,m+1))$ while $e_{2m}, m \geq 1$ are the edges $(\bullet(0,m), \circ(-1,m))$; see the left picture in Figure 4. We also remark that $\tilde{e}_{2m+1}$ and $\tilde{e}_{2m}$ are the edges $(\bullet(1,m+1), \circ(0,m+1))$ and $(\bullet(0,m), \circ(-1,m+1))$ for $m \geq 0$ respectively; see the right picture in Figure 4. Set $\Sigma_m = \{e_1, \ldots, e_m\}$ and $\tilde{\Sigma}_m = \{\tilde{e}_1, \ldots, \tilde{e}_m\}$ with the convention that $\tilde{\Sigma}_0 = \emptyset$.

4.1 Finite Graph

Consider a finite bipartite graph G contained in $\mathbb{Z}^2$ and set all edge weights to 1. Throughout this section, we denote $\mathbf{w}$ to be the vertex $\circ(-1,1)$ and $\mathbf{b}$ to be the vertex $\bullet(1,0)$. See Figure 5. With the notation of Definition 3.2 we have

Lemma 4.1. *For $l \geq 2$,*

$$\frac{Z_G[\{\mathbf{w},\mathbf{b}\}]}{Z_G} = \mathbb{P}_G[\tilde{e}_0, e_1] + \sum_{k=2}^{l} \mathbb{P}_G[\Sigma_k] + R_G^l, \tag{4.1}$$

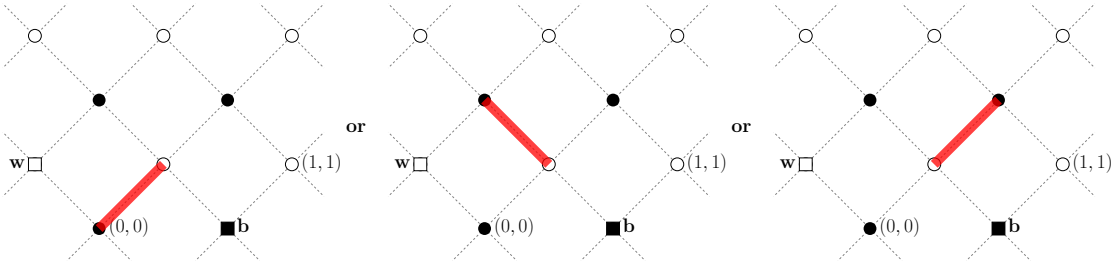

Figure 6: The three possible choices of dimers covering $\tilde{\mathbf{w}}$ on the graph $G\backslash\{\mathbf{w},\mathbf{b}\}$. The vertices $\mathbf{w}$ and $\mathbf{b}$ are depicted by squares to stress that they have been removed from the graph, together with the edges incident to them.

where

$$R_G^l = \frac{Z_G[\tilde{\Sigma}_{l-1}, \{\mathbf{w},\mathbf{b}\}]}{Z_G}. \tag{4.2}$$

and we assume that G is large enough to include Σ_l and $\tilde{\Sigma}_l$.

The above lemma and its proof have a similar flavour to [6, Proposition 3.5] with the key difference that $\mathbf{w}$ and $\mathbf{b}$ are not on the same face.

Proof. Consider the graph $G\backslash\{\mathbf{w},\mathbf{b}\}$. There are three possibilities for the dimers incident to the vertex $\tilde{\mathbf{w}} := \circ(0,1)$. These are given by the edges $(\bullet(0,0), \circ(0,1))$, $(\bullet(0,1), \circ(0,1))$ and $(\bullet(1,1), \circ(0,1)) = \tilde{e}_1$; see Figure 6. If a dimer covers the edge $(\bullet(0,0), \circ(0,1))$, then the remaining graph is the same as $G\backslash\{\tilde{e}_0, e_1\}$. If a dimer covers the edge $(\bullet(0,1), \circ(0,1))$ instead, the remaining graph is the same as $G\backslash\Sigma_2$. This gives (remember that all edge weights equal 1)

$$Z_G[\{\mathbf{w},\mathbf{b}\}] = Z_G[\{\tilde{e}_0, e_1\}] + Z_G[\Sigma_2] + Z_G[\tilde{\Sigma}_1, \{\mathbf{w},\mathbf{b}\}], \tag{4.3}$$

which can readily be seen from Figure 6.

For $m \geq 1$, we have inductively the equations

$$Z_G[\tilde{\Sigma}_{2m-1}, \{\mathbf{w},\mathbf{b}\}] = Z_G[\Sigma_{2m+1}] + Z_G[\tilde{\Sigma}_{2m}, \{\mathbf{w},\mathbf{b}\}], \tag{4.4}$$

and

$$Z_G[\tilde{\Sigma}_{2m}, \{\mathbf{w},\mathbf{b}\}] = Z_G[\Sigma_{2m+2}] + Z_G[\tilde{\Sigma}_{2m+1}, \{\mathbf{w},\mathbf{b}\}]. \tag{4.5}$$

Indeed, (4.4) follows because from the graph $G\backslash(\tilde{\Sigma}_{2m-1} \cup \{\mathbf{w},\mathbf{b}\})$, there are two possible dimers covering the vertex $\bullet(0,m)$: either the edge $(\bullet(0,m), \circ(0,m+1))$ is covered by a dimer or the edge $(\bullet(0,m), \circ(-1,m+1)) = \tilde{e}_{2m}$ is covered by a dimer; see Figure 7 for the case when $m = 1$. Then, (4.4) follows after noticing

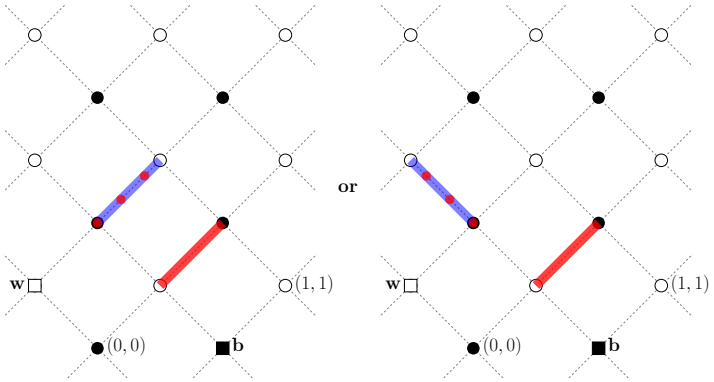

Figure 7: There are two choices of dimers, drawn in blue with a dotted red line overlaid, covering the vertex $\circ(0,1)$ given that the dimer in blue is already present on $G\backslash\{\mathbf{w},\mathbf{b}\}$. As in Figure 6, the vertices $\mathbf{w}$ and $\mathbf{b}$ are depicted by squares to stress that they have been removed from the graph. The left figure leads to first term on the right side of (4.4) while the right figure leads to the second term on the right side of (4.4).

that the graph $G\backslash(\tilde{\Sigma}_{2m-1}\cup\{(\bullet(0,m),\circ(0,m+1))\}\cup\{\mathbf{w},\mathbf{b}\})$ is the same as the graph $G\backslash\Sigma_{2m+1}$.

Similarly, to show (4.5), there are two possible dimers covering the vertex $\circ(0,m+1)$ which are $(\bullet(0,m+1),\circ(0,m+1))$ or $(\bullet(1,m+1),\circ(0,m+1)) = \tilde{e}_{2m+1}$. Then (4.5) follows after noticing that the graph $G\backslash(\tilde{\Sigma}_{2m}\cup\{(\bullet(0,m+1),\circ(0,m+1))\}\cup\{\mathbf{w},\mathbf{b}\})$ is the same as the graph $G\backslash\Sigma_{2m+2}$. We substitute the recursions in (4.4) and (4.5) into (4.3) to give

$$Z_G[\{\mathbf{w},\mathbf{b}\}] = Z_G[\{\tilde{e}_0,e_1\}] + Z_G[\tilde{\Sigma}_{l-1},\{\mathbf{w},\mathbf{b}\}] + \sum_{k=2}^{l} Z_G[\Sigma_k]. \tag{4.6}$$

We divide the above equation by Z_G and use the fact that $\mathbb{P}_G(\Sigma_k) = Z_G[\Sigma_k]/Z_G$. The claim is proved. □

Recall that K_G denotes the Kasteleyn matrix of G. If we want a Kasteleyn matrix for $G\backslash\{\mathbf{w},\mathbf{b}\}$, we cannot just take the restriction of K_G. The problem is that, since $\Phi(f_i) = -1$ for the four 1×1 square faces $f_1,\ldots,f_4$ of G around both $\mathbf{w}$ and $\mathbf{b}$ (recall (3.19) for the definition of $\Phi(f)$), for the 2×2 square faces $f_{\mathbf{w}}, f_{\mathbf{b}}$ that $G\backslash\{\mathbf{w},\mathbf{b}\}$ has around $\mathbf{w},\mathbf{b}$ we get $\Phi(f_{\mathbf{w}}) = \Phi(f_{\mathbf{b}}) = (-1)^4 = 1$ which does not satisfy (3.19). This is easily fixed: to define a valid Kasteleyn orientation on $G\backslash\{\mathbf{w},\mathbf{b}\}$ we need to reverse the orientation of a 'path of edges' connecting the two faces $f_{\mathbf{w}}, f_{\mathbf{b}}$. In our case, as we explain below, it is sufficient to reverse the

orientation of a single edge. A similar idea on a much more complicated scale was used in great success in [9] to find correlations in the monomer-dimer model.

We set $\tilde{\mathbf{w}}$ to be the vertex $\circ(0,1)$, $\mathbf{b_1}$ to be the vertex $\bullet(0,0)$, $\mathbf{b_2}$ to be the vertex $\bullet(0,1)$ and $\mathbf{b_3}$ to be the vertex $\bullet(1,1)$; see Figure 5. For simplicity, we organize the matrix K_G so that $\mathbf{w}$ and $\tilde{\mathbf{w}}$ are in columns 1 and 2 while $\mathbf{b_1}$, $\mathbf{b_2}$, $\mathbf{b_3}$ and $\mathbf{b}$ are in rows 1 to 4 (in that order).

Definition 4.2. *We let $K_G|_{V_1}$ be the matrix obtained from the matrix K_G by removing the rows and columns associated to the black and white vertices from V_1 respectively, for some collection of vertices $V_1 \subset V$.*

Further, define $\tilde{K}_G = \tilde{K}_G(b,w)$ for $w \in W_G \backslash \{\mathbf{w}\}$ and $b \in B_G \backslash \{\mathbf{b}\}$ by

$$\tilde{K}_G(b,w) = \begin{cases} K_G|_{\{\mathbf{b},\mathbf{w}\}}(b,w) & \text{if } (b,w) \neq (\mathbf{b_1}, \tilde{\mathbf{w}}), \\ -K_G(\mathbf{b_1}, \tilde{\mathbf{w}}) & \text{if } (b,w) = (\mathbf{b_1}, \tilde{\mathbf{w}}). \end{cases} \tag{4.7}$$

Observe that $\tilde{K}_G$ is a Kasteleyn matrix for $G \setminus \{\mathbf{w}, \mathbf{b}\}$, that satisfies (3.19).

The following lemma relates $\frac{Z_G[\mathbf{w},\mathbf{b}]}{Z_G}$ with entries of the inverse of K_G.

Lemma 4.3. *It holds*

$$\frac{Z_G[\{\mathbf{w},\mathbf{b}\}]}{Z_G} = \left| K_G^{-1}(\mathbf{w},\mathbf{b}) + \frac{2K_G(\mathbf{b_1},\tilde{\mathbf{w}})}{K_G(\mathbf{b_1},\mathbf{w})K_G(\mathbf{b},\tilde{\mathbf{w}})} \mathbb{P}_G[\tilde{e}_0, e_1] \right|. \tag{4.8}$$

Proof. The only nonzero entries of $\tilde{K}_G$ in the first column, which is indexed by the vertex $\tilde{\mathbf{w}}$, are the first three rows, which are indexed by the vertices $\mathbf{b_1}$, $\mathbf{b_2}$ and $\mathbf{b_3}$. Expanding out the determinant using the first column and noting (4.7) gives

$$\begin{aligned} \det \tilde{K}_G = &- K_G(\mathbf{b_1},\tilde{\mathbf{w}}) \det K_G|_{\{\mathbf{b},\mathbf{w},\mathbf{b_1},\tilde{\mathbf{w}}\}} - K_G(\mathbf{b_2},\tilde{\mathbf{w}}) \det K_G|_{\{\mathbf{b},\mathbf{w},\mathbf{b_2},\tilde{\mathbf{w}}\}} \\ &+ K_G(\mathbf{b_3},\tilde{\mathbf{w}}) \det K_G|_{\{\mathbf{b},\mathbf{w},\mathbf{b_3},\tilde{\mathbf{w}}\}}. \end{aligned} \tag{4.9}$$

Similarly, the matrix $K_G|_{\{\mathbf{b},\mathbf{w}\}}$, which corresponds to removing $\mathbf{b}$ and $\mathbf{w}$ from K_G, has the same nonzero entries in the first column as the matrix $\tilde{K}_G$. Expanding the determinant by the first column of $K_G|_{\mathbf{b},\mathbf{w}}$ gives

$$\begin{aligned} \det K_G|_{\{\mathbf{b},\mathbf{w}\}} = &K_G(\mathbf{b_1},\tilde{\mathbf{w}}) \det K_G|_{\{\mathbf{b},\mathbf{w},\mathbf{b_1},\tilde{\mathbf{w}}\}} - K_G(\mathbf{b_2},\tilde{\mathbf{w}}) \det K_G|_{\{\mathbf{b},\mathbf{w},\mathbf{b_2},\tilde{\mathbf{w}}\}} \\ &+ K_G(\mathbf{b_3},\tilde{\mathbf{w}}) \det K_G|_{\{\mathbf{b},\mathbf{w},\mathbf{b_3},\tilde{\mathbf{w}}\}}. \end{aligned} \tag{4.10}$$

Using the above two equations, we conclude that

$$\det \tilde{K}_G = \det K_G|_{\{\mathbf{b},\mathbf{w}\}} - 2K_G(\mathbf{b_1},\tilde{\mathbf{w}}) \det K_G|_{\{\mathbf{b},\mathbf{w},\mathbf{b_1},\tilde{\mathbf{w}}\}}. \tag{4.11}$$

We divide both sides of the above equation by $\det K_G$ and take absolute values of both sides which gives

$$\frac{Z_G[\{\mathbf{w},\mathbf{b}\}]}{Z_G} = \left|\frac{\det \tilde{K}_G}{\det K_G}\right| = \left|\frac{\det K_G|_{\{\mathbf{b},\mathbf{w}\}}}{\det K_G} - 2K_G(\mathbf{b_1},\tilde{\mathbf{w}})\frac{\det K_G|_{\{\mathbf{b},\mathbf{w},\mathbf{b_1},\tilde{\mathbf{w}}\}}}{\det K_G}\right|, \tag{4.12}$$

where we recall that $Z_G = |\det K_G|$, $Z_G[\{\mathbf{w},\mathbf{b}\}] = |\det \tilde{K}_G|$ by Kasteleyn's Theorem [12]. The claim then follows since $\det K_G|_{\{\mathbf{b},\mathbf{w}\}}/\det K_G = -K_G^{-1}(\mathbf{w},\mathbf{b})$ (recall that $\mathbf{w}$ and $\mathbf{b}$ are in the first column and fourth row of K_G) and due to

$$\begin{aligned} &2K_G(\mathbf{b_1},\tilde{\mathbf{w}})\frac{\det K_G|_{\{\mathbf{b},\mathbf{w},\mathbf{b_1},\tilde{\mathbf{w}}\}}}{\det K_G} \\ =&\frac{2K_G(\mathbf{b_1},\tilde{\mathbf{w}})}{K_G(\mathbf{b_1},\mathbf{w})K_G(\mathbf{b},\tilde{\mathbf{w}})}K_G(\mathbf{b_1},\mathbf{w})K_G(\mathbf{b},\tilde{\mathbf{w}})\frac{\det K_G|_{\{\mathbf{b},\mathbf{w},\mathbf{b_1},\tilde{\mathbf{w}}\}}}{\det K_G} \\ =&\frac{2K_G(\mathbf{b_1},\tilde{\mathbf{w}})}{K_G(\mathbf{b_1},\mathbf{w})K_G(\mathbf{b},\tilde{\mathbf{w}})}\mathbb{P}_G[\tilde{e}_0,e_1], \end{aligned} \tag{4.13}$$

because $|\det K_G| = Z_G$ and the overall signs match up for $\det K_G|_{\{\mathbf{b},\mathbf{w},\mathbf{b_1},\tilde{\mathbf{w}}\}}$ and $\det K_G$ [12]. □

The following corollary follows immediately from the statements of Lemmas 4.1 and 4.3.

Corollary 4.4. *We have*

$$\left|K_G^{-1}(\mathbf{w},\mathbf{b}) + \frac{2K_G(\mathbf{b_1},\tilde{\mathbf{w}})}{K_G(\mathbf{b_1},\mathbf{w})K_G(\mathbf{b},\tilde{\mathbf{w}})}\mathbb{P}_G[\tilde{e}_0,e_1]\right| = \mathbb{P}_G[\tilde{e}_0,e_1] + \sum_{k=2}^{l}\mathbb{P}_G[\Sigma_k] + R_G^l, \tag{4.14}$$

where R_G^l is given in (4.2).

Lemma 4.5. *We have*

$$0 \le R_G^l \le \mathbb{P}_G[e_1,\ldots,e_{l-1}]. \tag{4.15}$$

Proof. The lower bound is obvious since R_G^l is the ratio of two partition functions. We give the proof of the upper bound when $l-1=r$ is even; a similar argument holds for r odd.

Notice that the set of edges incident to $\tilde{\Sigma}_r \cup \{\mathbf{w},\mathbf{b}\}$ equals the set of edges incident to $\Sigma_r \cup \{\circ(-1,r/2+1),\bullet(1,r/2)\}$ and so we have that

$$\begin{aligned} Z_G[\tilde{\Sigma}_r,\{\mathbf{w},\mathbf{b}\}] &= Z_G[\Sigma_r,\{\circ(-1,r/2+1),\bullet(1,r/2)\}] \\ &= Z_{G\setminus\Sigma_r}[\{\circ(-1,r/2+1),\bullet(1,r/2)\}], \end{aligned} \tag{4.16}$$

where as usual $G\backslash\Sigma_r$ stands for the graph G with all incident edges to Σ_r removed, that is $Z_{G\backslash\Sigma_r} = Z_G[\Sigma_r]$. On the graph $G\backslash\Sigma_r$, the vertices $\circ(-1, r/2+1)$ and $\bullet(1, r/2)\}$ are on the same face. As is easily checked, this means that removing these vertices does not change the overall Kasteleyn orientation from $G\backslash\Sigma_r$. Hence, we have (recall the notation $K_G|_{V_1}$ from Definition 4.2)

$$\frac{Z_{G\backslash\Sigma_r}[\{\circ(-1, r/2+1), \bullet(1, r/2)\}]}{Z_{G\backslash\Sigma_r}} = \left|\frac{\det(K_{G\backslash\Sigma_r}|_{\{\bullet(1,r/2),\circ(-1,r/2+1)\}})}{\det(K_{G\backslash\Sigma_r})}\right| \leq 1. \quad (4.17)$$

The inequality holds because each term in the expansion of the determinant in the numerator is also present in the denominator. By noting that the denominator could have more terms and since all the terms in the expansion of the determinants have the same sign by Kasteleyn's theorem, the inequality follows. Multiplying both sides of the above inequality by $Z_{G\backslash\Sigma_r}$ and dividing both sides by Z_G gives the result. □

4.2 Infinite volume limit and proof of (2.6)

In this section, we extend the formula in Corollary 4.4 to the infinite volume limit:

Proposition 4.6. *Let $\bar{K}$ be the Kasteleyn matrix of $\mathbb{Z}^2$ defined in Section 3.1 and let B_1, B_2 be related to the slope ρ by (3.8) and (3.9). Then,*

$$\frac{e^{B_2}}{e^{B_1}}\left|\bar{K}^{-1}(\mathbf{w}, \mathbf{b}) + \frac{2\bar{K}(\mathbf{b_1}, \tilde{\mathbf{w}})}{\bar{K}(\mathbf{b_1}, \mathbf{w})\bar{K}(\mathbf{b}, \tilde{\mathbf{w}})}\pi_\rho^{\mathbb{Z}^2}[\tilde{e}_0, e_1]\right| = \pi_\rho^{\mathbb{Z}^2}[\tilde{e}_0, e_1] + \sum_{k=2}^{\infty}\pi_\rho^{\mathbb{Z}^2}[e_1, \ldots, e_k]. \quad (4.18)$$

Note that the sum that appears in the right side is the same as in the definition of average current, (3.14).

Proof of Proposition 4.6. We start from Corollary 4.4 and we take a graph G that tends to $\mathbb{Z}^2$ in such a way that around the vertices $\mathbf{w}, \mathbf{b}$ the dimer statistics $\mathbb{P}_G$ tends to that of $\pi_\rho^{\mathbb{Z}^2}$. Our choice for G is a suitable space translation of the so-called Aztec diamond: using the same coordinate system as above, the Aztec diamond A_L is a $L \times L$ subset of $\mathbb{Z}^2$ whose white vertices are given by $W_{A_L} := \{\circ(x, y) : 0 \leq x \leq L-1, 0 \leq y \leq L\}$, black vertices given by $B_{A_L} := \{\bullet(x, y) : 0 \leq x \leq L, 0 \leq y \leq L-1\}$ and whose edge set contains all the edges connecting W_{A_L} to B_{A_L}. As in Section 4.1 we assign weight 1 to all the edges of A_L. The Kasteleyn orientation we choose is $K_{A_L}(b, w) = 1$ for every vertical edge and $K_{A_L}(b, w) = i$ for every horizontal edge.

For uniformly random domino tilings of Aztec diamonds, the local behavior of the tiling separates, as $L \to \infty$, into two distinct macroscopic regions and the

interface between these two regions is referred to as the *limit shape* or *limit shape curve*. See [16] for a more complete overview: here we recall only what we need for our present work. Rescaling the Aztec diamond by L, so that the corners are given by $(0,0),(1,0),(1,1)$ and $(0,1)$, the limit shape is given by a circle of radius $1/2$ whose center is at $(1/2,1/2)$. We denote the open disk inside the circle by $\mathcal{D}$.

Fix $\xi = (\xi_1, \xi_2) \in \mathcal{D}$ and let G_L be the Aztec diamond A_L translated by $(-\lfloor \xi_1 L \rfloor, -\lfloor \xi_2 L \rfloor)$. Then, [7, Theorem 2.9] says that for any local dimer observable f, one has the convergence

$$\lim_{L\to\infty} \mathbb{P}_{G_L}(f) = \pi^{\mathbb{Z}^2}_{\hat{\rho}(\xi)}(f), \tag{4.19}$$

where $\hat{\rho}(\xi) := \rho(B(\xi))$, with $\rho(\cdot)$ as in (3.8)-(3.9) and $B = B(\xi) = (B_1(\xi), B_2(\xi))$ given by

$$B_i(\xi) = 1/2 \log(\xi_i/(1-\xi_i)). \tag{4.20}$$

Moreover, the inverse Kasteleyn matrix $K^{-1}_{A_L}$ satisfies, for every fixed pairs of vertices $(\circ(x_1,x_2), \bullet(y_1,y_2))$,

$$\lim_{L\to\infty} K^{-1}_{G_L}(\circ(x_1,x_2), \bullet(y_1,y_2)) = e^{B_1(y_1-x_1-1)} e^{B_2(y_2-x_2)} \overline{K}^{-1}(\circ(x_1,x_2), \bullet(y_1,y_2)), \tag{4.21}$$

To understand the exponential factor in the above formula, first notice that the left side of (4.21) is the inverse Kasteleyn matrix corresponding to a Kasteleyn weighting of $\mathbb{Z}^2$ with weights equal to 1 and i, while $\overline{K}^{-1}$ in the right side of (4.21) corresponds to $\mathbb{Z}^2$ having weights described by the Kasteleyn matrix in (3.5). The measures on each of these graphs are gauge equivalent (in the sense of Remark 3.3) as there is a gauge transformation from the graph corresponding to the left side of (4.21) to the graph corresponding to the right side of (4.21). More explicitly, this is given by multiplying the vertices $\bullet(y_1,y_2)$ by $e^{-B_2 y_2 - B_1 y_1}$ and the vertices $\circ(x_1,x_2)$ by $e^{B_1(x_1+1)+B_2 x_2}$. This explains the prefactor on the right side of (4.21). The convergence of $\lim_{L\to\infty} K^{-1}_{G_L}(\circ(x_1,x_2), \bullet(y_1,y_2))$ to its full plane counterpart is given in the proof of [7, Theorem 2.9]; see also Remark 4.7.

We will see in a moment that it is always possible to find $\xi \in \mathcal{D}$ such that $\hat{\rho}(\xi)$ equals the slope $\rho \in P^{\mathbb{Z}^2}$ that appears in (4.18). We have now all necessary ingredients to prove (4.18). We start from Corollary 4.4 with $G = G_L$. The probabilities $\mathbb{P}_{G_L}[\dots]$ tend as $L \to \infty$ to the corresponding $\pi^{\mathbb{Z}^2}_{\rho}$ probabilities by (4.19). The matrix element $K^{-1}_{G_L}(\mathbf{w}, \mathbf{b})$ tends, by (4.21), to

$$e^{B_2 - B_1} \overline{K}^{-1}(\mathbf{w}, \mathbf{b}), \tag{4.22}$$

while

$$\frac{K_{G_L}(\mathbf{b_1}, \tilde{\mathbf{w}})}{K_{G_L}(\mathbf{b_1}, \mathbf{w}) K_{G_L}(\mathbf{b}, \tilde{\mathbf{w}})} = -1 = e^{B_1 - B_2} \frac{\overline{K}(\mathbf{b_1}, \tilde{\mathbf{w}})}{\overline{K}(\mathbf{b_1}, \mathbf{w}) \overline{K}(\mathbf{b}, \tilde{\mathbf{w}})} \tag{4.23}$$

(recall (3.5) and the choice of Kasteleyn matrix for the Aztec diamond, which is just as in (3.5) with $B_1 = B_2 = 0$). Finally, by Lemma 4.5 we see that

$$0 \leq \limsup_{L\to\infty} R^l_{G_L} \leq \pi_\rho^{\mathbb{Z}^2}[e_1, \ldots, e_{l-1}], \tag{4.24}$$

so that, letting $l \to \infty$ we obtain (4.18) (we have already remarked in Section 3.2.1 that the series is convergent).

It remains only to prove that the image of the map $\xi \in \mathcal{D} \mapsto \hat{\rho}(\xi)$ is the whole open square $P^{\mathbb{Z}^2}$. In fact, it is easy to verify that the map $\xi \mapsto (B_1, B_2), B_i = 1/2 \log(\xi_i/(1-\xi_i))$ gives a one-to-one correspondence between $\mathcal{D}$ and the amoeba $\mathcal{B}$ defined in (3.11) and we already mentioned that the map $B \in \mathcal{B} \mapsto \rho(B) \in P^{\mathbb{Z}^2}$ in (3.8)-(3.9) is also a bijection. □

Remark 4.7. *For simplicity, the weights on A_L were chosen to be* 1 *and* i. *The Kasteleyn matrix for the Aztec diamond in the uniform case in [7] differs by K_{A_L} only up to sign, which means entries of the inverse differ up to a sign.*

The proof of [7, Theorem 2.9] involves showing the convergence of the entries of $K^{-1}_{G_L}$ as L tends to infinity. Note that this limiting inverse Kasteleyn matrix is an inverse of a Kasteleyn matrix different from the one we considered in this paper given in (3.5)*; the two are gauge equivalent. We believe that the choice in this paper is more natural and aesthetically pleasing, mainly because the slopes are embedded into the edge weights, which mirrors the honeycomb case.*

Proof of Theorem 2.3. We now compute the speed of growth for dynamics on $\mathbb{Z}^2$. Recalling formula (3.14) for the speed and Proposition 4.6, we see that

$$v^{\mathbb{Z}^2}(\rho) = \frac{e^{B_2}}{e^{B_1}} \left| \bar{K}^{-1}(\mathbf{w}, \mathbf{b}) + \frac{2\bar{K}(\mathbf{b_1}, \tilde{\mathbf{w}})}{\bar{K}(\mathbf{b_1}, \mathbf{w})\bar{K}(\mathbf{b}, \tilde{\mathbf{w}})} \pi_\rho^{\mathbb{Z}^2}[\tilde{e}_0, e_1] \right| - \pi_\rho^{\mathbb{Z}^2}[\tilde{e}_0, e_1] + \pi_\rho^{\mathbb{Z}^2}[\tilde{e}_0^c, e_1], \tag{4.25}$$

where $\tilde{e}_0^c$ is the event that the edge $\tilde{e}_0$ is not present. The result (2.6) then follows immediately from Lemma A.4 in Appendix A. □

5 Large time height fluctuations on $\mathcal{H}$

Remark 5.1. *The Gibbs measure $\pi_\rho^{\mathcal{H}}$ is invariant under translations and reflection through the center of any hexagonal face. In fact, such transformations clearly preserve the Gibbs property (the measure is locally uniform, conditioned on the configuration outside any finite domain) and leave the three dimer densities unchanged. Given that the Gibbs measure with given densities is unique, the claim follows. Note that, under reflection, the function $V(e)$ transforms into $\widehat{V}(e')$ for some e' that depends on the face chosen as center of reflection. Here, $\widehat{V}(e)$ is the*

number of hexagonal faces that the lowest *horizontal dimer* above e *has to cross in order to reach* e *(*$\widehat{V}(e)=0$ *if the move is not allowed).*

Recall that Theorem 2.4 follows by proving the equilibrium estimate (3.16). For $i\in\{0,1\}$, let Λ_L^i denote the set of horizontal edges $e=(\bullet(x{+}1,n),\circ(x,n{+}1))\in\Lambda_L$ with $x \bmod 2 = i$, i.e., those in even (for $i=0$) or odd (for $i=1$) columns. By Cauchy-Schwarz and Remark 5.1 we have

$$\begin{aligned}\mathrm{Var}_{\pi_\rho^{\mathcal{H}}}\Big(\sum_{e\in\Lambda_L} V(e)\Big) &= \mathrm{Var}_{\pi_\rho^{\mathcal{H}}}\Big(\sum_{e\in\Lambda_L^0}\widehat{V}(e)+\sum_{e\in\Lambda_L^1}\widehat{V}(e)\Big)\\ &\le 2\mathrm{Var}_{\pi_\rho^{\mathcal{H}}}\Big(\sum_{e\in\Lambda_L^0}\widehat{V}(e)\Big)+2\mathrm{Var}_{\pi_\rho^{\mathcal{H}}}\Big(\sum_{e\in\Lambda_L^1}\widehat{V}(e)\Big).\end{aligned}\tag{5.1}$$

Proposition 5.2. *For* $i\in\{0,1\}$*, we have for some constant* $C(\rho)>0$

$$\mathrm{Var}_{\pi_\rho^{\mathcal{H}}}\Big(\sum_{e\in\Lambda_L^i}\widehat{V}(e)\Big)=\sum_{e_1,e_2\in\Lambda_L^i}\pi_\rho^{\mathcal{H}}(\widehat{V}(e_1);\widehat{V}(e_2))\le CL^2\log L,\tag{5.2}$$

with $\pi(f;g):=\pi(fg)-\pi(f)\pi(g)$ *(the covariance of* f *and* g*).*

The proof is given in Section 5.3. The advantage of the decomposition (5.1) is that in (5.2) terms with e_1,e_2 in neighboring columns, that would require a special treatment, do not appear. In most figures of this section we find it convenient to deform the hexagonal faces of $\mathcal{H}$ into rectangles, as in the drawing on the right of Figure 1, so that the axes $\hat{e}_1,\hat{e}_2$ become orthogonal.

Given the horizontal edge $e=(\bullet(x+1,n),\circ(x,n+1))$, define the edge set

$$O_{m,e}=\bigcup_{i=0}^{m-1}\{(\bullet(x,n{+}i{+}1),\circ(x,n{+}1{+}i)),(\bullet(x{+}1,n{+}i),\circ(x{+}1,n{+}i{+}1))\}\tag{5.3}$$

and

$$\tilde{O}_{m,e}=\bigcup_{i=1}^{m}\{(\bullet(x,n{+}1{-}i),\circ(x,n{+}1{-}i)),(\bullet(x{+}1,n{-}i),\circ(x{+}1,n{+}1{-}i))\}\tag{5.4}$$

for $m\ge 1$. Using the notation $e+m=(\bullet(x+1,n+m),\circ(x,n+1+m))$, $m\in\mathbb{Z}$, we have $O_{m,e}=\widetilde{O}_{m,e+m}$. Also, we define

$$\widetilde{V}(e)=\sum_{m\ge1}\mathbb{1}_{\widetilde{O}_{m,e}}.\tag{5.5}$$

5.1 Expressions for $\pi_\rho^{\mathcal{H}}(\widetilde{V}(e_1);\widetilde{V}(e_2))$

We first determine a more explicit expression for $\widehat{V}(e)$, which was defined in Remark 5.1. We use the notation that $\mathbb{1}_{O_{m,e}}$ means the indicator event of dimers covering the edges $O_{m,e}$. Setting $B_{m,e} = O_{m,e} \cup \{(\bullet(x+1, n+m), \circ(x, n+m+1))\}$, and by considering the possible dimers incident to the vertex $\bullet(x+1, n+m)$, we have

$$\mathbb{1}_{O_{m,e}} = \mathbb{1}_{B_{m,e}} + \mathbb{1}_{O_{m+1,e}}. \tag{5.6}$$

By definition of $\widehat{V}(e)$ and the above equation

$$\widehat{V}(e) = \sum_{m=1}^{\infty} m\mathbb{1}_{B_{m,e}} = \sum_{m=1}^{\infty} m(\mathbb{1}_{O_{m,e}} - \mathbb{1}_{O_{m+1,e}}) = \sum_{m=1}^{\infty} \mathbb{1}_{O_{m,e}}. \tag{5.7}$$

By linearity and translation invariance, $\pi_\rho^{\mathcal{H}}[\widehat{V}(e)] = \pi_\rho^{\mathcal{H}}[\widetilde{V}(e)]$. As shown in [6], the expectation of $\widetilde{V}(e)$ can be written in terms of a single entry of $\overline{K}^{-1}$, namely

$$\pi_\rho^{\mathcal{H}}[\widetilde{V}(e)] = -\frac{a_2 a_3}{a_1}\overline{K}^{-1}(\circ(x+1, n), \bullet(x, n)). \tag{5.8}$$

Extending the ideas of [6], in Proposition 5.4 we derive a formula for a 2×2 determinant of $\overline{K}^{-1}$ in terms of $\widetilde{O}_{m,e}$. This will be almost the same as $\pi_\rho^{\mathcal{H}}(\widetilde{V}(e_1);\widetilde{V}(e_2))$. Then, in Section 5.3, we will express the variance (5.2) in terms of correlations $\pi_\rho^{\mathcal{H}}(\widetilde{V}(e_1);\widetilde{V}(e_2))$.

Proposition 5.3. *For $j \in \{1, 2\}$ consider the horizontal edges $e_j = (\bullet(x_j + 1, n_j), \circ(x_j, n_j + 1))$ with $x_1, x_2, n_1, n_2 \in \mathbb{Z}$.*
If $|x_1 - x_2| > 1$, then

$$\pi_\rho^{\mathcal{H}}[\widetilde{V}(e_1)\widetilde{V}(e_2)] = \sum_{m_1,m_2=1}^{\infty} \pi_\rho^{\mathcal{H}}[\widetilde{O}_{m_1,e_1}\,\widetilde{O}_{m_2,e_2}]. \tag{5.9}$$

If $x_1 = x_2$ and $n_1 > n_2$, then

$$\pi_\rho^{\mathcal{H}}[\widetilde{V}(e_1)\widetilde{V}(e_2)] = \sum_{m_1=1}^{|n_1-n_2|-1}\sum_{m_2=1}^{\infty} \pi_\rho^{\mathcal{H}}[\widetilde{O}_{m_1,e_1}\,\widetilde{O}_{m_2,e_2}] + \sum_{m=1}^{\infty} 2m\,\pi_\rho^{\mathcal{H}}[\widetilde{O}_{|n_1-n_2|+m,e_1}]. \tag{5.10}$$

The case $x_1 = x_2$ and $n_2 < n_1$ is obtained by symmetry. Finally, if $e_1 = e_2$, then

$$\pi_\rho^{\mathcal{H}}[\widetilde{V}(e_1)\widetilde{V}(e_2)] = \sum_{m=1}^{\infty}(2m-1)\pi_\rho^{\mathcal{H}}[\widetilde{O}_{m,e_1}]. \tag{5.11}$$

Convergence of the sums is shown later.

Proof. The statement for $|x_1 - x_2| > 1$ simply follows from (5.5).

For $e_1 = e_2$, using $\mathbb{1}_{\widetilde{O}_{m_1,e_1}} \mathbb{1}_{\widetilde{O}_{m_2,e_1}} = \mathbb{1}_{\widetilde{O}_{\max\{m_1,m_2\},e_1}}$, we get

$$\widetilde{V}(e_1)\widetilde{V}(e_2) = \sum_{m=1}^{\infty} \mathbb{1}_{\widetilde{O}_{m,e_1}} + 2\sum_{m_2=2}^{\infty}\sum_{m_1=1}^{m_2-1} \mathbb{1}_{\widetilde{O}_{m_2,e_1}} = \sum_{m=1}^{\infty}(2m-1)\mathbb{1}_{\widetilde{O}_{m,e_1}}. \tag{5.12}$$

For $x_1 = x_2$, we suppose that $n_1 > n_2$. The result for $n_1 < n_2$ is recovered by relabeling. We have

$$\widetilde{V}(e_1)\widetilde{V}(e_2) = \sum_{m_1=1}^{|n_1-n_2|-1}\sum_{m_2=1}^{\infty} \mathbb{1}_{\widetilde{O}_{m_1,e_1}}\mathbb{1}_{\widetilde{O}_{m_2,e_2}} + \sum_{m_1=|n_1-n_2|}^{\infty}\sum_{m_2=1}^{\infty} \mathbb{1}_{\widetilde{O}_{m_1,e_1}}\mathbb{1}_{\widetilde{O}_{m_2,e_2}}. \tag{5.13}$$

For the last term, the two $\widetilde{O}$ join so that $\mathbb{1}_{\widetilde{O}_{m_1,e_1}}\mathbb{1}_{\widetilde{O}_{m_2,e_2}} = \mathbb{1}_{\widetilde{O}_{\max\{m_1,m_2+|n_1-n_2|\},e_1}}$. Using this, the second term in (5.13) becomes

$$\sum_{m=1}^{\infty} 2m\mathbb{1}_{\widetilde{O}_{m+|n_1-n_2|,e_1}}. \tag{5.14}$$

Taking expectations with respect to $\pi_\rho^{\mathcal{H}}$ finishes the proof. □

5.2 Expressions involving $\overline{K}^{-1}$

Recall that $\overline{K}^{-1}$ represents the inverse Kasteleyn matrix on $\mathcal{H}$ whose entries are given by (3.4).

Proposition 5.4. *Let $e_i = (\bullet(x_i+1, n_i), \circ(x_i, n_i+1))$ for $i = 1, 2$. Then,*

$$\begin{aligned}
&\frac{(a_2a_3)^2}{a_1^2}\det\left(\overline{K}^{-1}(\circ(x_i+1,n_i),\bullet(x_j,n_j))\right)_{1\le i,j\le 2} \\
&= \begin{cases} \displaystyle\sum_{m_1=1}^{\infty}\sum_{m_2=1}^{\infty} \pi_\rho^{\mathcal{H}}[\tilde{O}_{m_1,e_1}\tilde{O}_{m_2,e_2}] & \text{if } |x_1-x_2|>1, \\ \displaystyle\sum_{m_1=1}^{|n_1-n_2|-1}\sum_{m_2=1}^{\infty} \pi_\rho^{\mathcal{H}}[\tilde{O}_{m_1,e_1}\tilde{O}_{m_2,e_2}] + \sum_{m=1}^{\infty}\pi_\rho^{\mathcal{H}}[\tilde{O}_{m+|n_1-n_2|,e_1}] & \text{if } x_1=x_2,\ n_1>n_2. \end{cases}
\end{aligned} \tag{5.15}$$

The case $x_1 = x_2, n_2 > n_1$ can be obtained by symmetry; for $x_1 = x_2, n_1 = n_2$ the determinant is zero.

To prove Proposition 5.4 we first obtain a similar expression of a finite subgraph $H = (V_H, E_H)$ of the honeycomb grid which admits a dimer covering, where however the sums needs to have a cut-off and a remainder. After taking the limit $H \to \mathcal{H}$ and removing the cut-off, one recovers Proposition 5.4. Edge weights on H are chosen to be identically 1.

For the statement on H we define the following subsets of vertices: for $m \geq 1$

$$\check{\Sigma}_{m,x,n} = \bigcup_{i=0}^{m-1} \{\bullet(x, n-i), \circ(x, n-i), \bullet(x+1, n-i-1), \circ(x+1, n-i)\} \quad (5.16)$$

with $\check{\Sigma}_{0,x,n} = \emptyset$, and for $m \geq 0$

$$\Sigma_{m,x,n} = \check{\Sigma}_{m,x,n} \cup \{\bullet(x, n-m), \circ(x+1, n-m)\}. \quad (5.17)$$

Recall the notation $Z_G[V, E]$ from Definition 3.2.

Proposition 5.5. *Let e_1, e_2 be as in Proposition 5.4 and let N_1, N_2 be positive integers. Assume that the graph H includes all vertices and edges appearing in the expressions below. We have that* $\det\left[(K_H)^{-1}(\circ(x_i+1, n_i), \bullet(x_j, n_j))\right]_{1\leq i,j\leq 2}$ *equals*

$$\sum_{m_1=1}^{N_1} \sum_{m_2=1}^{N_2} \mathbb{P}_H[\tilde{O}_{m_1,e_1} \tilde{O}_{m_2,e_2}] + R_1^H \quad (5.18)$$

if $|x_1 - x_2| > 1$ and

$$\sum_{m_1=1}^{|n_1-n_2|-1} \sum_{m_2=1}^{N_2} \mathbb{P}_H[\tilde{O}_{m_1,e_1} \tilde{O}_{m_2,e_2}] + \sum_{m_2=1}^{N_2} \mathbb{P}_H[\tilde{O}_{m_2+|n_1-n_2|,e_1}] + R_0^H \quad (5.19)$$

if $x_1 = x_2$ and $n_1 > n_2$. The case $x_1 = x_2$ and $n_2 > n_1$ can be obtained by symmetry.

The remainder terms $R_i^H = R_i^H(x_1, n_1, N_1, x_2, n_2, N_2)$ for $i \in \{0, 1\}$ are given by:

$$\begin{aligned} Z_H R_1^H(x_1, n_1, N_1, x_2, n_2, N_2) &= Z_H[\Sigma_{N_1,x_1,n_1} \cup \Sigma_{N_2,x_2,n_2}] \\ &+ \sum_{m_2=1}^{N_2} Z_H[\Sigma_{N_1,x_1,n_1} \cup \check{\Sigma}_{m_2,x_2,n_2}] + \sum_{m_1=1}^{N_1} Z_H[\check{\Sigma}_{m_1,x_1,n_1} \cup \Sigma_{N_2,x_2,n_2}], \end{aligned} \quad (5.20)$$

and

$$\begin{aligned} Z_H R_0^H(x, n_1, N_1, x, n_2, N_2) = \sum_{m_1=1}^{|n_1-n_2|-1} & Z_H[\check{\Sigma}_{m_1,x,n_1} \cup \Sigma_{N_2,x,n_2}] \\ & + Z_H[\Sigma_{|n_1-n_2|+N_2,x,n_1}]. \end{aligned} \quad (5.21)$$

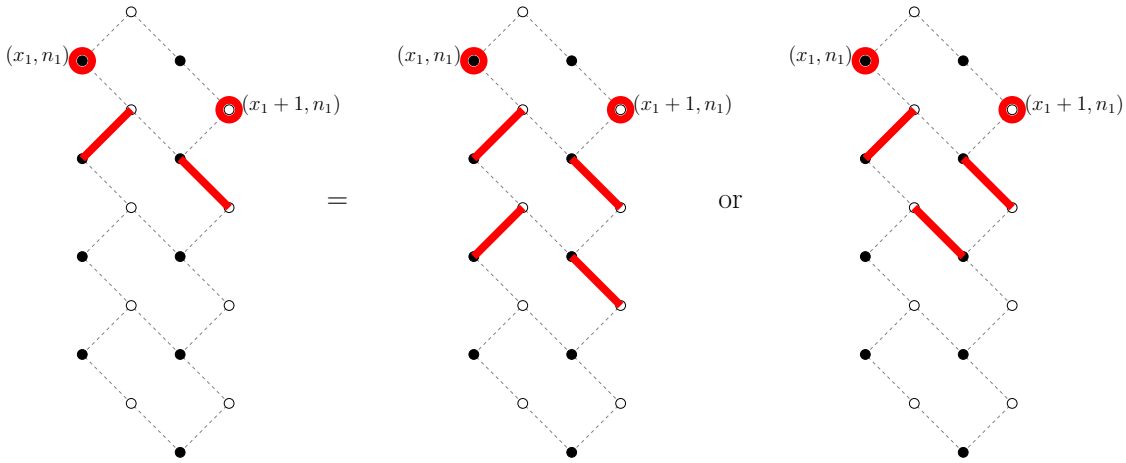

Figure 8: Vertices incident to red circles or red edges are those that are removed from the graph. The removed vertices on the left side are given by Σ_{1,x_1,n_1}. By considering the dimers incident to $\circ(x_1, n_1 - 1)$, this gives Σ_{2,x_1,n_1} or $\check{\Sigma}_{2,x_1,n_1}$.

Proof. Consider the graph $H\backslash(\Sigma_{0,x_1,n_1} \cup \Sigma_{0,x_2,n_2})$. The vertices removed from H are on the same face (for each pair). This means that the Kasteleyn orientation of $H\backslash(\Sigma_{0,x_1,n_1} \cup \Sigma_{0,x_2,n_2})$ is the same as that of H (up to the removed vertices and their incident edges). An equivalent viewpoint is adding auxiliary edges between $\circ(x_i+1, n_i)$ and $\bullet(x_i, n_i)$ which must be covered by dimers for $i \in \{1, 2\}$, and each auxiliary edge having orientation from $\circ(x_i+1, n_i)$ to $\bullet(x_i, n_i)$ for $i \in \{1, 2\}$. This means that $Z_H[\Sigma_{0,x_1,n_1}]/Z_H = -(K_H)^{-1}(\circ(x_1+1, n_1), \bullet(x_1, n_1))$ and

$$\frac{Z_H[\Sigma_{0,x_1,n_1} \cup \Sigma_{0,x_2,n_2}]}{Z_H} = \det\left[K_H^{-1}(\circ(x_i+1, n_i), \bullet(x_j, n_j))\right]_{1\le i,j\le 2}. \tag{5.22}$$

Case 1: $|x_1 - x_2| > 1$. We manipulate the dimer possibilities on $H\backslash(\Sigma_{0,x_1,n_1} \cup \Sigma_{0,x_2,n_2})$. Consider $H\backslash(\Sigma_{m_1,x_1,n_1} \cup \Sigma_{0,x_2,n_2})$ and the possible dimers incident to $\bullet(x_1, n - m_1)$; this leads to

$$Z_H[\Sigma_{m_1,x_1,n_1} \cup \Sigma_{0,x_2,n_2}] = Z_H[\Sigma_{m_1+1,x_1,n_1} \cup \Sigma_{0,x_2,n_2}] + Z_H[\check{\Sigma}_{m_1+1,x_1,n_1} \cup \Sigma_{0,x_2,n_2}], \tag{5.23}$$

noting that $\Sigma_{m_1,x_1,n_1} \cup \{\bullet(x_1+1, n_1 - m_1 - 1), \circ(x_1, n_1 - m_1)\}$ is the same as $\check{\Sigma}_{m_1+1,x_1,n_1}$; see Figure 8. Iterating (5.23) gives

$$Z_H[\Sigma_{0,x_1,n_1} \cup \Sigma_{0,x_2,n_2}] = Z_H[\Sigma_{N_1,x_1,n_1} \cup \Sigma_{0,x_2,n_2}] + \sum_{m_1=1}^{N_1} Z_H[\check{\Sigma}_{m_1,x_1,n_1} \cup \Sigma_{0,x_2,n_2}]. \tag{5.24}$$

Since the set Σ_{m_2,x_2,n_2} for $0 \le m_2 \le N_2$ does not intersect Σ_{m_1,x_1,n_1} for $0 \le m_1 \le N_1$, applying an analogous procedure given above to $Z_H[\Sigma_{N_1,x_1,n_1} \cup \Sigma_{0,x_2,n_2}]$ and

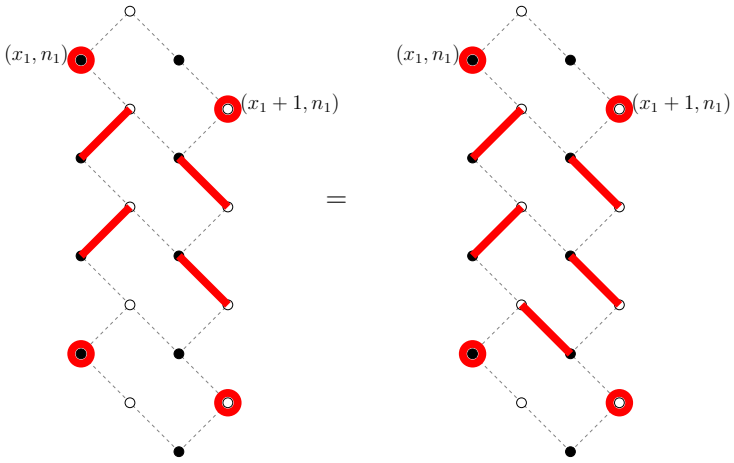

Figure 9: Using the same conventions as in Figure 8, the left side shows $\Sigma_{2,x_1,n_1} \cup \Sigma_{0,x_2,n_2}$ removed from the graph with $x_1 - x_2 = 0$ and $n_1 = n_2 + 3$. The right side shows the same configuration but with the edge that is forced to be covered by a dimer.

$Z_H[\check{\Sigma}_{m_1,x_1,n_1} \cup \Sigma_{0,x_2,n_2}]$ gives

$$Z_H[\Sigma_{0,x_1,n_1} \cup \Sigma_{0,x_2,n_2}] = R_1^H Z_H + \sum_{m_1=1}^{N_1} \sum_{m_2=1}^{N_2} Z_H[\check{\Sigma}_{m_1,x_1,n_1} \cup \check{\Sigma}_{m_2,x_2,n_2}], \tag{5.25}$$

where R_1^H is as given in the statement of the proposition. Dividing both sides of the above equation by Z_H, noting (5.22) and

$$\frac{Z_H[\check{\Sigma}_{m_1,x_1,n_1} \cup \check{\Sigma}_{m_2,x_2,n_2}]}{Z_H} = \mathbb{P}_H[\tilde{O}_{m_1,e_1} \tilde{O}_{m_2,e_2}] \tag{5.26}$$

gives (5.18).

Case 2: $x_1 = x_2 \equiv x$. We give the computation for $n_1 > n_2$ because the computation is similar for $n_1 < n_2$. By noting that there is a single choice of dimer incident to the vertex $\circ(x, n_2+1)$ on the graph $H \backslash (\Sigma_{|n_1-n_2|-1,x,n_1} \cup \Sigma_{m_2,x,n_2})$ which is given by the edge $(\circ(x, n_2+1), \bullet(x+1, n_2))$, that $\Sigma_{|n_1-n_2|-1,x,n_1} \cup \{\circ(x, n_2+1), \bullet(x+1, n_2)\} = \check{\Sigma}_{|n_1-n_2|,x,n_1}$, and that $\Sigma_{|n_1-n_2|,x,n_1} \cup \Sigma_{m_2,x,n_2} = \Sigma_{|n_1-n_2|+m_2,x,n_1}$,

then by following the steps given for $|x_1 - x_2| > 1$, we have

$$Z_H[\Sigma_{0,x,n_1} \cup \Sigma_{0,x,n_2}] = \sum_{m_1=1}^{|n_1-n_2|-1} Z_H[\check{\Sigma}_{m_1,x,n_1} \cup \Sigma_{N_2,x,n_2}] + \sum_{m_2=1}^{N_2} Z_H[\check{\Sigma}_{|n_1-n_2|+m_2,x,n_1}] + Z_H[\Sigma_{|n_1-n_2|+N_2,x,n_1}] + \sum_{m_1=1}^{|n_1-n_2|-1} \sum_{m_2=1}^{N_2} Z_H[\check{\Sigma}_{m_1,x,n_1} \cup \check{\Sigma}_{m_2,x,n_2}]. \tag{5.27}$$

Dividing both sides of the above equation by Z_H, noting (5.22) and

$$\frac{Z_H[\check{\Sigma}_{|n_1-n_2|+m_2,x,n_1}]}{Z_H} = \mathbb{P}_H[\tilde{O}_{m_2+|n_1-n_2|,e_1}] \tag{5.28}$$

leads to (5.19). □

Proof of Proposition 5.4. The first step is to provide bounds for R_0^H and R_1^H in terms of probabilities. This is achieved by using the same argument given in Lemma 4.5 to each of the terms found in these expressions. That is, we have that

$$Z_H[\Sigma_{N_1,x_1,n_1} \cup V] \leq Z_H[\check{\Sigma}_{N_1,x_1,n_1} \cup V], \tag{5.29}$$

where V denotes a set of removed vertices which are not incident to the edges incident to Σ_{N_1,x_1,n_1}. To verify this equation, recall that $\Sigma_{N_1,x_1,n_1} = \check{\Sigma}_{N_1,x_1,n_1} \cup \{\bullet(x_1, n_1 - N_1), \circ(x_1 + 1, n_1 - N_1)\}$. Since the two additional vertices are on the same face, the Kasteleyn orientation on the graphs $H\backslash(\Sigma_{N_1,x_1,n_1} \cup V)$ and $H\backslash(\check{\Sigma}_{N_1,x_1,n_1} \cup V)$ are the same up to these two additional vertices, which means that

$$\frac{Z_H[\Sigma_{N_1,x_1,n_1} \cup V]}{Z_H[\check{\Sigma}_{N_1,x_1,n_1} \cup V]} = \frac{\det(K_{H\backslash(\check{\Sigma}_{N_1,x_1,n_1} \cup V)}|_{\bullet(x_1,n_1-N_1),\circ(x_1+1,n_1-N_1)})}{\det(K_{H\backslash(\check{\Sigma}_{N_1,x_1,n_1} \cup V)})} \leq 1 \tag{5.30}$$

because each term in the expansion of the determinant in the numerator is also present in the denominator. We show how to use the above inequalities to bound each of the terms in R_0^H and R_1^H by using the term $Z_H[\Sigma_{N_1,x_1,n_1} \cup \Sigma_{N_2,x_2,n_2}]/Z_H$ as an example. The rest of the terms follow by similar computations. From (5.29) and (5.26) we obtain

$$\frac{Z_H[\Sigma_{N_1,x_1,n_1} \cup \Sigma_{N_2,x_2,n_2}]}{Z_H} \leq \mathbb{P}_H[\tilde{O}_{N_1,e_1}\tilde{O}_{N_2,e_2}]. \tag{5.31}$$

Using this and analogous bounds we can estimate the error terms R_0^H, R_1^H as

$$0 \leq R_1^H \leq \mathbb{P}_H[\tilde{O}_{N_1,e_1}\tilde{O}_{N_2,e_2}] + \sum_{m_2=1}^{N_2} \mathbb{P}_H[\tilde{O}_{N_1,e_1}\tilde{O}_{m_2,e_2}] + \sum_{m_1=1}^{N_1} \mathbb{P}_H[\tilde{O}_{m_1,e_1}\tilde{O}_{N_2,e_2}] \tag{5.32}$$

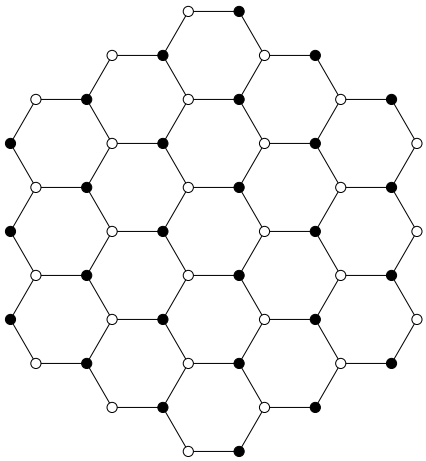

Figure 10: The hexagonal graph H_L for $L = 3$.

and

$$0 \leq R_0^H \leq \sum_{m_1=1}^{|n_1-n_2|-1} \mathbb{P}_H[\tilde{O}_{m_1,e_1}\tilde{O}_{N_2,e_2}] + \mathbb{P}_H[\tilde{O}_{|n_1-n_2|+N_2,e_1}]. \tag{5.33}$$

For the moment we did not specify the finite graph H: now we take it to be a $L \times L \times L$ hexagonal subset $H = H_L$ of $\mathcal{H}$ (see Figure 10 for $L = 3$). Non-zero entries $K_{H_L}(b, w)$ of its Kasteleyn matrix are chosen to be all equal to 1. We will let L grow to infinity and, in a second stage, we will let N_1, N_2 in Proposition 5.5 tend to infinity.

Similar to uniform random tilings of Aztec diamonds, uniform dimer coverings of a large hexagon exhibit a limit shape phenomenon [8], that we briefly recall. Rescale H_L by a factor $1/L$ so that it converges to a hexagon H_∞ of side length 1 as $L \to \infty$ and let $\mathcal{D} \subset H_\infty$ be the open disk tangent to the six sides of H_∞. Let $\xi \in \mathcal{D}$ and let $\hat{H}_L$ be the graph H_L translated by $-\lfloor \xi L \rfloor$. Then, Theorem 2 in [20] says that the local statistics under $\mathbb{P}_{\hat{H}_L}$ converges to that of a Gibbs measure $\pi^{\mathcal{H}}_{\hat{\rho}}$, for a certain (rather explicit) $\hat{\rho} = \hat{\rho}(\xi_1, \xi_2) \in P^{\mathcal{H}}$. Moreover, Proposition 7.10 in [20] implies that the inverse Kasteleyn matrix $K^{-1}_{\hat{H}_L}$ satisfies, for any fixed vertices $\circ(x_1, x_2), \bullet(y_1, y_2)$,

$$\lim_{L\to\infty} K^{-1}_{\hat{H}_L}(\circ(x_1, x_2), \bullet(y_1, y_2)) = a_2 \left(\frac{a_1}{a_3}\right)^{y_1-x_1} \left(\frac{a_2}{a_3}\right)^{y_2-x_2} \overline{K}^{-1}(\circ(x_1, x_2), \bullet(y_1, y_2)). \tag{5.34}$$

This is the analog of (4.21) for the square lattice. Here, $\overline{K}^{-1}$ is the infinite inverse Kasteleyn matrix (3.4), with $a_i = a_i(\hat{\rho})$ (recall that edge weights are a function

of the slope, as discussed just before (3.4)). As in (4.21), the exponential prefactors in the r.h.s. arise from the gauge transformation relating the Kasteleyn matrix $K_{\hat{H}_L}$, with weights 1, to that of the infinite lattice $\mathcal{H}$, with weights a_1, a_2, a_3. Moreover, for every $\rho \in P^{\mathcal{H}}$ it is possible to find $\xi \in \mathcal{D}$ such that $\hat{\rho}(\xi) = \rho$, and this is how we fix ξ.

Note that Petrov's results hold for more general regions than hexagonal ones, but we do not need this level of generality here.

We let $L \to \infty$ now. From (5.34) we see that

$$\lim_{L\to\infty} \det\Big(K^{-1}_{\hat{H}_L}(\circ(x_i+1,n_i),\bullet(x_j,n_j))\Big)_{1\le i,j\le 2} = \frac{(a_2a_3)^2}{a_1^2}\det\Big(\overline{K}^{-1}(\circ(x_i+1,n_i),\bullet(x_j,n_j))\Big)_{1\le i,j\le 2}. \quad (5.35)$$

Also, from the above discussion we see that all the $\mathbb{P}_{\hat{H}_L}$ probabilities in (5.18) and (5.19) tend to the corresponding $\pi^{\mathcal{H}}_\rho$ probabilities, while (recall (5.33))

$$0 \le \liminf_{L\to\infty} R_0^{\hat{H}_L} \le \limsup_{L\to\infty} R_0^{\hat{H}_L} \le \sum_{m_1=1}^{|n_1-n_2|-1} \pi^{\mathcal{H}}_\rho[\tilde{O}_{m_1,e_1}\tilde{O}_{N_2,e_2}] + \pi^{\mathcal{H}}_\rho(\tilde{O}_{|n_1-n_2|+N_2,e_1}), \quad (5.36)$$

and a similar bound for $R_1^{\hat{H}_L}$ from (5.32).

Thus we have shown that $\frac{(a_2a_3)^2}{a_1^2}\det\left((K^{-1}(\circ(x_i+1,n_i),\bullet(x_j,n_j))\right)_{1\le i,j\le 2}$, which is independent of N_1 and N_2, it is a sum of non-negative terms. This implies that the sums are convergent and consequently the remainder terms tends to zero as N_1 and N_2 tend to infinity (this can be deduced also from Eq. (5.37) below). The statement of Proposition 5.4 follows. □

Remark 5.6. *The above proof uses a hexagonal finite graph H_L and the convergence of its inverse Kasteleyn matrix to that of $\mathcal{H}$. The approach to compute the speed of growth used in the published version of [6](Proposition 3.7) uses instead a toroidal graph T_L with $L \to \infty$ but it contains mistakes since it does not take into account the fact that on the torus the terms in the expansion of the determinant of K_{T_L} come with different signs. Although that argument could be adjusted, it is much simpler to use the planar hexagonal graph H_L instead, as we do here.*

5.3 Proof of Proposition 5.2

The two variance terms on the right side of (5.1) are bounded in the same way. We therefore presents the details for only one. Recall that Λ^0_L consists of all horizontal edges $e = (\bullet(x+1,n), \circ(x,n+1))$ with $x, n \in [0, L]$ and even x. For several bounds

we will use (this can be deduced from Lemma A.1 of [23])

$$\pi_\rho^{\mathcal{H}}(O_{m,e}) = \pi_\rho^{\mathcal{H}}(\widetilde{O}_{m,e}) \leq C_1 e^{-c_1 m} \tag{5.37}$$

where $C_1, c > 0$ are constants depending on ρ.

Recall that $\widehat{V}(e) = \sum_{m\geq 1} \mathbb{1}_{O_{m,e}}$ and $\widetilde{V}(e) = \sum_{m\geq 1} \mathbb{1}_{\widetilde{O}_{m,e}}$. Also, we define

$$D(e) = \sum_{\substack{m\geq 1:\\ \widetilde{O}_{m,e}\not\subset\Lambda_L^0}} \mathbb{1}_{\widetilde{O}_{m,e}}, \quad U(e) = \sum_{\substack{m\geq 1:\\ O_{m,e}\not\subset\Lambda_L^0}} \mathbb{1}_{O_{m,e}}. \tag{5.38}$$

Recall that $O_{m_i,e_i} = \widetilde{O}_{m_i,e_i+m_i}$ and notice the following bijection: for (m,e) such that $O_{m,e} \subset \Lambda_L^0$, there exists a unique pair $(\tilde{m},\tilde{e})$ such that $O_{m,e} = \widetilde{O}_{\tilde{m},\tilde{e}}$, namely $\tilde{m} = m$ and $\tilde{e} = e + m$ (and vice versa). This gives

$$\sum_{e\in\Lambda_L^0} \widehat{V}(e) = \sum_{e\in\Lambda_L^0} \widetilde{V}(e) + \sum_{e\in\Lambda_L^0} U(e) - \sum_{e\in\Lambda_L^0} D(e). \tag{5.39}$$

By Cauchy-Schwarz, it is enough to bound the variances of the three sums above. Let us first bound the variance of the sum of $U(e)$. Bounding the variance by the second moment we get

$$\mathrm{Var}_{\pi_\rho^{\mathcal{H}}}\Big(\sum_{e\in\Lambda_L^0} U(e)\Big) \leq \sum_{e_1,e_2\in\Lambda_L^0} \sum_{\substack{m_1,m_2\geq 1:\\ O_{m_1,e_1}\not\subset\Lambda_L^0\\ O_{m_2,e_2}\not\subset\Lambda_L^0}} \pi_\rho^{\mathcal{H}}(O_{m_1,e_1}O_{m_2,e_2}). \tag{5.40}$$

Using (5.37), $\pi_\rho^{\mathcal{H}}(O_{m_1,e_1}O_{m_2,e_2}) \leq \min\{\pi_\rho^{\mathcal{H}}(O_{m_1,e_1}), \pi_\rho^{\mathcal{H}}(O_{m_2,e_2})\}$ and $\min\{e^{-cx}, e^{-cy}\} \leq e^{-c(x+y)/2}$ for $x, y \geq 0$, we get

$$(5.40) \leq \Bigg(C_1 \sum_{e\in\Lambda_L^0} \sum_{\substack{m\geq 1:\\ O_{m,e}\not\subset\Lambda_L^0}} e^{-c_1 m/2}\Bigg)^2 = \mathcal{O}(L^2). \tag{5.41}$$

Similarly one gets the bound for the variance of $\sum_{e\in\Lambda_L^0} D(e)$.

For the main term, we have

$$\mathrm{Var}_{\pi_\rho^{\mathcal{H}}}\Big(\sum_{e\in\Lambda_L^0} \widetilde{V}(e)\Big) = \sum_{e_1,e_2\in\Lambda_L^0} \Big(\pi_\rho^{\mathcal{H}}[\widetilde{V}(e_1)\widetilde{V}(e_2)] - \pi_\rho^{\mathcal{H}}[\widetilde{V}(e_1)]\pi_\rho^{\mathcal{H}}[\widetilde{V}(e_2)]\Big). \tag{5.42}$$

Using (5.8) we have

$$\sum_{e_1,e_2\in\Lambda_L^0} \pi_\rho^{\mathcal{H}}[\widetilde{V}(e_1)]\pi_\rho^{\mathcal{H}}[\widetilde{V}(e_2)] = \sum_{e_1,e_2\in\Lambda_L^0} \left(\frac{a_2 a_3}{a_1}\right)^2 \prod_{i=1}^{2} \overline{K}^{-1}(\circ(x_i+1,n_i), \bullet(x_i,n_i)). \tag{5.43}$$

Propositions 5.3 and 5.4 imply that

$$\sum_{e_1,e_2\in\Lambda_L^0}\pi_\rho^{\mathcal{H}}[\widetilde{V}(e_1)\widetilde{V}(e_2)] = E_\Lambda + \sum_{e_1,e_2\in\Lambda_L^0}\left(\frac{a_2a_3}{a_1}\right)^2 \det\Big[\overline{K}^{-1}(\circ(x_i+1,n_i),\bullet(x_j,n_j))\Big]_{1\le i,j\le 2} \tag{5.44}$$

where the error term E_Λ is given by

$$E_\Lambda = \sum_{\substack{e_1,e_2\in\Lambda_L^0;\\ x_1=x_2}}\sum_{m\ge 1}(2m-1)\pi_\rho^{\mathcal{H}}[\widetilde{O}_{m+|n_2-n_1|,e_1\vee e_2}] \tag{5.45}$$

and $e_1\vee e_2 = e_1\mathbb{1}_{n_1>n_2} + e_2\mathbb{1}_{n_1<n_2}$. We recall that $e_j = (\bullet(x_j+1,n_j),\circ(x_j,n_j+1))$ as in Proposition 5.3. Plugging (5.43) and (5.44) into (5.42) leads to

$$\mathrm{Var}_{\pi_\rho^{\mathcal{H}}}\Big(\sum_{e\in\Lambda_L^0}\widetilde{V}(e)\Big) = E_\Lambda + \sum_{e_1,e_2\in\Lambda_L^0}\left(\frac{a_2a_3}{a_1}\right)^2\prod_{i=1}^{2}\overline{K}^{-1}(\circ(x_i+1,n_i),\bullet(x_{i+1},n_{i+1})), \tag{5.46}$$

with $x_3\equiv x_1$ and $n_3\equiv n_1$. Thus it remains to bound the two terms in (5.46).

The leading term is bounded as follows. We have

$$\Big|\overline{K}^{-1}(\circ(x_i+1,n_i),\bullet(x_{i+1},n_{i+1}))\Big| \le \frac{C}{1+|n_1-n_2|+|x_1-x_2|}, \tag{5.47}$$

where $C=C(\rho)$. The above bound follows from the computations given in the proof of Lemma 4.4 in [17]. We omit details. Thus we have

$$\begin{aligned}&\sum_{e_1,e_2\in\Lambda_L^0}\Big|\prod_{i=1}^{2}\overline{K}^{-1}(\circ(x_i+1,n_i),\bullet(x_{i+1},n_{i+1}))\Big| \\ &\le \sum_{x_1,n_1,x_2,n_2\in[0,L]}\frac{C'}{1+|n_1-n_2|^2+|x_1-x_2|^2} \le C''L^2\log L\end{aligned} \tag{5.48}$$

as wished. Finally, using (5.37), E_Λ is bounded by

$$C_1\sum_{\substack{e_1,e_2\in\Lambda_L^0;\\ x_1=x_2}}\sum_{m\ge 1}(2m-1)e^{-c_1(m+|n_1-n_2|)} = \mathcal{O}(L^2). \tag{5.49}$$

This completes the proof of Proposition 5.2.

A Formulas on $\mathbb{Z}^2$

In this section, we give formulas useful for the inverse Kasteleyn matrix on $\mathbb{Z}^2$.

Lemma A.1. *For $\mathcal{G} = \mathbb{Z}^2$ and provided that $|\tanh B_2 \cosh B_1| \leq 1$ then*

$$\overline{K}^{-1}(\circ(x_1, x_2), \bullet(y_1, y_2)) = \frac{f(x_1, x_2, y_1, y_2)}{2\pi \mathrm{i}} \int_C \frac{z^{y_1 - x_1 - 1}(z-1)^{y_2 - x_2}}{(z+1)^{y_2 - x_2 + 1}} dz \qquad \text{(A.1)}$$

where $f(x_1, x_2, y_1, y_2) = \mathrm{i}^{y_1 - x_1 + x_2 - y_2 - 1} e^{B_2(y_2 - x_2)} e^{B_1(y_1 - x_1 - 1)}$ and C is a contour from $\overline{\Omega}_c$ to $\Omega_c = e^{-B_1} e^{\mathrm{i} \arccos(\cosh(B_1)\tanh(B_2))}$ passing to the right of the origin if $y_2 \geq x_2$ and passing to the left of the origin if $y_2 < x_2$.

Note that the condition $|\tanh B_2 \cosh B_1| \leq 1$ is the one that defines the amoeba $\mathcal{B}$ in (3.11).

Proof of Lemma A.1. In (3.6), we make the change of variables $z_1 \mapsto z_1 e^{B_1}$ and $z_2 \mapsto z_2 e^{B_2}$ which gives

$$\overline{K}^{-1}(\circ(x_1, x_2), \bullet(y_1, y_2)) = \frac{e^{B_1(y_1 - x_1 - 1) + B_2(y_2 - x_2)}}{(2\pi \mathrm{i})^2} \int \frac{dz_1}{z_1} \frac{dz_2}{z_2} \frac{z_1^{y_1 - x_1 - 1} z_2^{y_2 - x_2}}{1 + \mathrm{i} z_1^{-1} + \mathrm{i} z_2^{-1} + z_1^{-1} z_2^{-1}} \qquad \text{(A.2)}$$

for $w = \circ(x_1, x_2), b = \bullet(y_1, y_2)$ where the integral are over positive contours $|z_1| = e^{-B_1}$ and $|z_2| = e^{-B_2}$.

We make the change of variables $\omega = (\mathrm{i} - z_2)/(\mathrm{i} + z_2)$ (i.e., $z_2 = -\mathrm{i}(\omega - 1)/(1 + \omega)$) and $z_1 = z\mathrm{i}$ which gives

$$\frac{f(x_1, x_2, y_1, y_2)}{(2\pi \mathrm{i})^2} \int dz \int d\omega \frac{(\omega - 1)^{y_2 - x_2}}{(\omega + 1)^{y_2 - x_2 + 1}} \frac{1}{\omega - z}, \qquad \text{(A.3)}$$

where the contour for $|z| = e^{-B_1}$ is positively oriented and the contour for ω is explained below. Taking the residue at $\omega = z$ gives the integral described in the lemma. It remains to find the contours under these transformations, ascertain that there are no other contributions, and finally verify the intersection points.

The map $\omega = (\mathrm{i} - z_2)/(\mathrm{i} + z_2)$ maps the positively oriented contour $|z_2| = e^{-B_2}$ to:

(a) for $B_2 > 0$, to a positively oriented circle having positive real part, center on the real axis, and including 1,

(b) for $B_2 = 0$, to the imaginary line from $\infty\mathrm{i}$ to $-\infty\mathrm{i}$,

(c) for $B_2 < 0$, to a negatively oriented circle having negative real part, center on the real axis, and including -1.

In particular, these contours intersect with $|z| = e^{-B_1}$ if and only if $|\tanh B_1 \cosh B_2| \leq 1$. From now we consider this restriction of the values of B_1, B_2. The two intersections are complex conjugate complex numbers Ω_c and $\overline{\Omega}_c$, with the convention that $\mathrm{Im}(\Omega_c) \geq 0$. A simple geometric computation gives $\Omega_c = e^{-B_1} e^{\mathrm{i} \arccos(\cosh(B_1)\tanh(B_2))}$.

Notice that the possible poles in ω are $\omega = z$ and $\omega = \pm 1$. The residue at infinity is zero and therefore, by Cauchy residue's theorem, for any value of B_2 we can choose to perform the integral over ω:

(A) either along a positively oriented path enclosing the poles at 1 and at the portion of z from $\overline{\Omega}_c$ to Ω_c,

(B) or along a negatively oriented path enclosing the poles at -1 and at the portion of z from Ω_c to $\overline{\Omega}_c$.

The idea is now to choose between option (A) and (B) for the contours in such a way that the poles at ± 1 are never inside the contour for ω, so that we are left (at most) with the pole at z only.

Case 1: $y_2 - x_2 \geq 0$. In this case there is a pole at -1 and we choose the contour for ω as in (A). The residue at $\omega = z$ gives the claimed result.

Case 2: $y_2 - x_2 < 0$. In this case there is a pole at 1 and we choose the contour for ω as in (B). The residue at $\omega = z$ gives, due to the orientation of the contour, -1 times the integral over z from Ω_c to $\overline{\Omega}_c$, which can be equivalently be though to be the integral over z from $\overline{\Omega}_c$ to Ω_c passing to the left of the origin. □

Lemma A.2. *For $\mathcal{G} = \mathbb{Z}^2$ and provided that $|\tanh(B_2)\cosh(B_1)| \leq 1$*

$$\rho_1 = -\frac{1}{2} + \frac{1}{\pi} \arg \Omega_c \tag{A.4}$$

and

$$\rho_2 = \frac{\arg(\Omega_c - 1)}{\pi} - \frac{\arg(\Omega_c + 1)}{\pi} - \frac{1}{2} \tag{A.5}$$

where Ω_c is defined in Lemma A.1.

Proof. Using the integral formula for $\overline{K}^{-1}$ found in Lemma A.1, we have from (3.8)

$$\begin{aligned} \rho_1 &= \frac{1}{2} - \frac{1}{2\pi} \int \left(\frac{\mathrm{i}}{\omega - 1} - \frac{\mathrm{i}}{(\omega - 1)\omega} \right) d\omega \\ &= \frac{1}{2} - \frac{1}{2\pi} \int \frac{\mathrm{i}}{\omega} d\omega, \end{aligned} \tag{A.6}$$

where the integral goes between $\overline{\Omega}_c$ and Ω_c and passes to the left of the origin. The formula for ρ_1 follows from evaluating the above integral. The formula for ρ_2 follows from a similar computation.

□

Lemma A.3. *For $\mathcal{G} = \mathbb{Z}^2$ provided that $|\tanh(B_2)\cosh(B_1)| \leq 1$ then*

$$\overline{K}^{-1}(\circ(-1,1), \bullet(1,0)) = \frac{e^{B_1-B_2}\left(-\arg\left(\Omega_c - 1\right) - \operatorname{Im}\left(\Omega_c\right) + \pi\right)}{\pi}, \tag{A.7}$$

and

$$\overline{K}^{-1}(\circ(0,1), \bullet(1,0)) = -\frac{\mathrm{i}e^{-B_2}\left(\pi - \arg\left(\Omega_c - 1\right)\right)}{\pi}. \tag{A.8}$$

Proof. These follow from evaluating the appropriate single integral formulas from Lemma A.1. □

Lemma A.4. *We have that*

$$\begin{aligned}&\frac{1}{e^{B_1-B_2}}\left(\bar{K}^{-1}(\mathbf{w},\mathbf{b}) + 2\frac{\bar{K}(\mathbf{b_1},\tilde{\mathbf{w}})}{\bar{K}(\mathbf{b_1},\mathbf{w})\bar{K}(\mathbf{b},\tilde{\mathbf{w}})}\pi_\rho^{\mathbb{Z}^2}[\tilde{e}_0, e_1]\right) + \frac{\mathrm{Im}\Omega_c}{\pi} \\ &= -\pi_\rho^{\mathbb{Z}^2}[\tilde{e}_0, e_1] + \pi_\rho^{\mathbb{Z}^2}[\tilde{e}_0^c, e_1],\end{aligned} \tag{A.9}$$

$$-\pi_\rho^{\mathbb{Z}^2}[\tilde{e}_0, e_1] + \pi_\rho^{\mathbb{Z}^2}[\tilde{e}_0^c, e_1] - \frac{\mathrm{Im}\Omega_c}{\pi} < 0, \tag{A.10}$$

and

$$\mathrm{Im}\Omega_c = \frac{\sin^2\psi_1}{\tan\psi_2} + \frac{\sin\psi_1}{\sin\psi_2}\sqrt{\sin^2\psi_2 + \sin^2\psi_1\cos^2\psi_2} \tag{A.11}$$

where Ω_c is defined in Lemma A.1, $\psi_i = (1/2 + \rho_i)\pi$ for $i \in \{1,2\}$.

Proof. By noticing that

$$\frac{2}{e^{B_1-B_2}}\frac{\bar{K}(\mathbf{b_1},\tilde{\mathbf{w}})}{\bar{K}(\mathbf{b_1},\mathbf{w})\bar{K}(\mathbf{b},\tilde{\mathbf{w}})} = \frac{2}{e^{B_1-B_2}}\frac{e^{B_1+B_2}}{\mathrm{i}^2 e^{2B_2}} = -2 \tag{A.12}$$

and

$$-\pi_\rho^{\mathbb{Z}^2}[\tilde{e}_0, e_1] + \pi_\rho^{\mathbb{Z}^2}[\tilde{e}_0^c, e_1] = -2\pi_\rho^{\mathbb{Z}^2}[\tilde{e}_0, e_1] + \pi_\rho^{\mathbb{Z}^2}[e_1], \tag{A.13}$$

the first equation follows by comparing $\frac{1}{e^{B_1-B_2}}\bar{K}^{-1}(\circ(-1,1), \bullet(1,0))$ and $\pi_\rho^{\mathbb{Z}^2}[e_1] = \overline{K}(\bullet(1,0), \circ(0,1))\overline{K}^{-1}(\circ(0,1), \bullet(1,0)) = (\mathrm{i}e^{B_2})\overline{K}^{-1}(\circ(0,1), \bullet(1,0))$ which are both given in Lemma A.3.

To verify (A.10), we have using Lemma A.3 and (3.2) to compute $\pi_\rho^{\mathbb{Z}^2}[\tilde{e}_0, e_1]$

$$\begin{aligned}&\frac{1}{e^{B_1-B_2}}\left(\bar{K}^{-1}(\mathbf{w},\mathbf{b}) + 2\frac{\bar{K}(\mathbf{b_1},\tilde{\mathbf{w}})}{\bar{K}(\mathbf{b_1},\mathbf{w})\bar{K}(\mathbf{b},\tilde{\mathbf{w}})}\pi_\rho^{\mathbb{Z}^2}[\tilde{e}_0, e_1]\right) \\ &= -\frac{(\pi - \arg(\Omega_c - 1))(\pi - 2\arg(\Omega_c))}{\pi^2} - \frac{\pi - 2\arg(\Omega_c - 1) + 2\arg(\Omega_c)}{\pi^2}\mathrm{Im}\Omega_c.\end{aligned} \tag{A.14}$$

Denote by $Q = -\pi^2$(A.14). Let $\Omega_c = re^{\mathrm{i}\theta}$ and $\phi = \phi(r,\theta) = \arg(\Omega_c - 1)$. First notice that $\lim_{r\to 0} Q = 0$ since $\phi \to \pi$. To see (A.10) it is thus enough to verify $\frac{dQ}{dr} \geq 0$. Using $\frac{d\phi}{dr} = -\frac{\sin\theta}{|\Omega_c - 1|^2}$ we have

$$\frac{dQ}{dr} = \frac{\sin\theta}{|\Omega_c - 1|^2} P, \text{ with } P = \pi - 2\theta + 2r\sin\theta + (\pi + 2\theta - 2\phi)|\Omega_c - 1|^2. \quad \text{(A.15)}$$

If we see that $P \geq 0$, then also $\frac{dQ}{dr} \geq 0$. Now, $\lim_{r\to 0} P = 0$, thus it is enough to verify $\frac{dP}{dr} \geq 0$. Using $\frac{d|\Omega_c - 1|^2}{dr} = 2(r - \cos\theta)$, we have

$$\frac{dP}{dr} = 4\sin\theta + 2(\pi + 2\theta - 2\phi)(r - \cos\theta). \quad \text{(A.16)}$$

For $\theta \in [\pi/2, \pi)$, $\phi - \theta < \pi/2$ and thus both terms in (A.16) are positive. For $\theta \in [0, \pi/2)$, $\pi + 2\theta - 2\phi$ and $r - \cos\theta$ are both increasing in r with $\lim_{r\to 0}(\pi + 2\theta - 2\phi) = 2\theta - \pi < 0$ and $\lim_{r\to 0}(r - \cos\theta) = -\cos\theta < 0$. Also, at $r = \cos\theta$ one has $\pi + 2\theta - 2\phi = 0$. This implies that both term in the rhs. of (A.16) are positive, ending the proof of (A.10).

Finally, to find $\mathrm{Im}\Omega_c$ notice that from Lemma A.2 we have $\arg\Omega_c = \psi_1 = (\rho_1 + 1/2)\pi$ and

$$\psi_2 = (\rho_2 + 1/2)\pi = \arg(\Omega_c - 1) - \arg(\Omega_c + 1) = \arg((\Omega_c - 1)/(\Omega_c + 1)) \quad \text{(A.17)}$$

from which $\tan\psi_2 = 2\frac{\mathrm{Im}\Omega_c}{|\Omega_c|^2 - 1}$. By using $|\Omega_c|\sin\psi_1 = \mathrm{Im}\Omega_c$ we have

$$\tan\psi_2 = 2\frac{\mathrm{Im}\Omega_c}{(\frac{\mathrm{Im}\Omega_c}{\sin\psi_1})^2 - 1}, \quad \text{(A.18)}$$

and we can solve for $\mathrm{Im}\Omega_c$ as required. □

B Hessian of the speed of growth for square lattice

To verify that the model belongs to the anisotropic KPZ class of growth models in $2+1$ dimensions, one needs to verify that the determinant of the Hessian of $v^{\mathbb{Z}^2}$ is ≤ 0. To do this, consider the speed of growth as function of $\psi_1, \psi_2 \in [0,\pi]^2$ given in (2.6). Denote by $\mathrm{Hess}(\psi_1,\psi_2)$ the Hessian of $v^{\mathbb{Z}^2}(\psi_1,\psi_2)$. An explicit (a bit lengthy) computation gives that det(Hess) equals

$$W(\psi_1,\theta) = \frac{-5 - e^{4\theta}(2 + e^{2\theta})^2 + 2e^{2\theta}[(2 + e^{2\theta})\cos(4\psi_1) + 4(1 + \sinh(2\theta))\cos(2\psi_1)]}{(2\cosh(\theta))^4} \quad \text{(B.1)}$$

where we used the variables $\sinh(\theta) := \sin(\psi_1)/\tan(\psi_2)$. Now θ spans all $\mathbb{R}$. For any fixed $\theta \in \mathbb{R}$, we have that $W(\psi_1, \theta) = W(\pi - \psi_1, \theta)$, thus we can restrict to $\psi_1 \in [0, \pi/2]$.

A computation gives

$$\begin{aligned} W(0,\theta) &= -\frac{(e^{4\theta} + 2e^{2\theta} - 3)^2}{(2\cosh(\theta))^4} \leq 0 \text{ with } = 0 \text{ only for } \theta = 0, \\ W(\pi/2,\theta) &= -4e^{4\theta} < 0, \\ W(\psi_1, -\infty) &= 0, \quad W(\psi_1, \infty) = -\infty. \end{aligned} \tag{B.2}$$

Thus at the boundary of the domain for ψ_1 and θ the Hessian is ≤ 0. Assume that there is a point inside the domain where $W > 0$. Then there is a maximum inside the domain where $\frac{dW}{d\psi_1} = \frac{dW}{d\theta} = 0$. The only possible solutions of $\frac{dW}{d\psi_1} = 0$ for $\psi_1 \in (0, \pi/2)$ is $\cos(\psi_1) = \zeta := \cosh(\theta)/\sqrt{2 + e^{2\theta}}$. With this value of ψ_1, we have however $\frac{dW}{d\theta} = -\frac{8e^{5\theta}\cosh(\theta)(3+2\cosh(2\theta))}{(2+e^{2\theta})^2} < 0$. Thus there is no maximum for $(\psi_1, \theta) \in (0, \pi/2) \times (-\infty, \infty)$.

References

[1] A. Borodin, I. Corwin, and P.L. Ferrari. Anisotropic (2+1)d growth and gaussian limits of q-whittaker processes. *Probab. Theory Rel. Fields (Online First)*, *preprint: arXiv:1612:00321*, 2016.

[2] A. Borodin, I. Corwin, and F.L. Toninelli. Stochastic heat equation limit of a $(2 + 1)$D growth model. *Commun. Math. Phys.* **350**:957-984, 2017

[3] A. Borodin and P.L. Ferrari. Anisotropic KPZ growth in $2 + 1$ dimensions: fluctuations and covariance structure. *J. Stat. Mech.*, page P02009, 2009.

[4] A. Borodin and P.L. Ferrari. Anisotropic Growth of Random Surfaces in $2+1$ Dimensions. *Comm. Math. Phys.*, 325:603–684, 2014.

[5] A. Borodin and S. Shlosman. Gibbs ensembles of nonintersecting paths. *Commun. Math. Phys.* **293**, 145-170, 2010.

[6] S. Chhita and P.L. Ferrari. A combinatorial identity for the speed of growth in an anisotropic KPZ model, *Ann. Inst. Henri Poincaré D* **4**, 453-477, 2017.

[7] S. Chhita, K. Johansson, and B. Young. Asymptotic domino statistics in the Aztec diamond. *Ann. Appl. Probab.*, 25(3):1232–1278, 2015.

[8] H. Cohn, M. Larsen, and J. Propp. The shape of a typical boxed plane partition. *New York J. Math.*, 4:137–165, 1998.

[9] J. Dubédat. Dimers and families of Cauchy-Riemann operators I. *J. Amer. Math. Soc.*, 28(4):1063–1167, 2015.

[10] M. Duits. The Gaussian free field in an interlacing particle system with two jump rates. *Comm. Pure Appl. Math.*, 66:600–643, 2013.

[11] T. Halpin-Healy and A. Assdah. On the kinetic roughening of vicinal surfaces. *Phys. Rev. A*, 46:3527–3530, 1992.

[12] P.W. Kasteleyn. The statistics of dimers on a lattice : I. The number of dimer arrangements on a quadratic lattice. *Physica*, 27:1209–1225, 1961.

[13] P.W. Kasteleyn. Dimer statistics and phase transitions. *J. Math. Phys.*, 4:287–293, 1963.

[14] R. Kenyon. Local statistics of lattice dimers. *Ann. Inst. H. Poincaré Probab. Statist.*, 33(5):591–618, 1997.

[15] R. Kenyon. Height fluctuations in the honeycomb dimer model. *Comm. Math. Phys.*, 281:675–709, 2008.

[16] R. Kenyon. Lectures on dimers. In *Statistical mechanics*, volume 16 of *IAS/Park City Math. Ser.*, pages 191–230. Amer. Math. Soc., Providence, RI, 2009.

[17] R. Kenyon, A. Okounkov, and S. Sheffield. Dimers and amoebae. *Ann. of Math.*, 163:1019–1056, 2006.

[18] H.J. Kim, I. Kim, and J.M. Kim. Hybridized discrete model for the anisotropic Kardar-Parisi-Zhang equation. *Phys. Rev. E*, 58:1144–1147, 1998.

[19] B. Laslier and F.L. Toninelli. How quickly can we sample a uniform domino tiling of the $2L \times 2L$ square via Glauber dynamics? *Probability Theory and Related Fields*, 161(3-4):509–559, 2015.

[20] L. Petrov. Asymptotics of random lozenge tilings via Gelfand-Tsetlin schemes. *Probab. Theory Related Fields*, 160(3-4):429–487, 2014.

[21] M. Prähofer and H. Spohn. An Exactly Solved Model of Three Dimensional Surface Growth in the Anisotropic KPZ Regime. *J. Stat. Phys.*, **88**:999–1012, 1997.

[22] H.N.V. Temperley and M.E. Fisher. Dimer problem in statistical mechanics—an exact result. *Philos. Mag. (8)*, 6:1061–1063, 1961.

[23] F.L. Toninelli. A $(2+1)$-dimensional growth process with explicit stationary measures. *Ann. Probab.*, **45**: 2899-2940, 2017.

[24] D.E. Wolf. Kinetic roughening of vicinal surfaces. *Phys. Rev. Lett.*, 67:1783–1786, 1991.